Summertime surface PM_1 aerosol composition and size by source region at the Lampedusa island in the central Mediterranean Sea

Marc D. Mallet[1,2,3], Barbara D'Anna[2,4], Aurélie Même[2,*], Maria Chiara Bove[5,6], Federico Cassola[5,7], Giandomenico Pace[8], Karine Desboeufs[1], Claudia Di Biagio[1], Jean-Francois Doussin[1], Michel Maille[1], Dario Massabò[5], Jean Sciare[9], Pascal Zapf[1], Alcide Giorgio di Sarra[8] and Paola Formenti[1]

1. LISA, CNRS UMR7583, Université Paris Est Créteil (UPEC), Université de Paris , Institut Pierre Simon Laplace (IPSL), Créteil, France

2. IRCELYON, CNRS UMR 5652, Univ. Lyon1, Lyon, France

3. Centre National d'Etudes Spatiales (CNES), Toulouse, France

4. LCE, CNRS UMR 7376, Aix-Marseille Université, Marseille, France

5. Department of Physics & INFN, University of Genoa, Genoa, Italy

6. ARPAL Physical Agents and Air Pollution Sector, La Spezia, Italy

7. ARPAL CFMI-PC, Genoa, Italy (current affiliation)

8. Laboratory for Observations and Analyses of Earth and Climate, ENEA, Rome, Italy

9. The Cyprus Institute, Energy, Environment and Water Research Center, Nicosia, Cyprus

*now at Bruker

For submission to the ChArMex special issue in Atmos. Chem. Phys.

Abstract

Measurements of aerosol composition and size distributions were taken during the summer of 2013 at the remote island of Lampedusa in the southern central Mediterranean Sea. These measurements were part of the ChArMEx/ADRIMED (Chemistry and Aerosol Mediterranean Experiment/Aerosol Direct Radiative Forcing on the Mediterranean Climate) framework and took place during the Special Observation Period 1a (SOP-1a) from 11 June until 5 July 2013.

From compact time-of-flight aerosol mass spectrometer (cToF-AMS) measurements in the size range below 1 µm in aerodynamic diameter (PM_1), particles were predominately comprised of ammonium and sulphate. On average, ammonium sulphate contributed 63% to the non-refractory PM_1 mass, followed by organics (33%). The organic aerosol was generally very highly oxidised (f_{44} values were typically between 0.25 and 0.26). The contribution of ammonium

sulphate was generally higher than organic aerosol in comparison to measurements taken in the western Mediterranean but is consistent with studies undertaken in the eastern basin.

Source apportionment of organics using a statistical (positive matrix factorisation) model revealed four factors; a hydrocarbon-like organic aerosol (HOA), a methanesulfonic acid related oxygenated organic aerosol (MSA-OOA), a more oxidised oxygenated organic aerosol (MO-OOA) and a less oxidised oxygenated organic aerosol we label (LO-OOA). The MO-OOA was the dominant factor for most of the campaign (53% of the PM_1 OA mass). It was well correlated with SO_4^{2-}, highly oxidised, and generally more dominant during easterly air masses originating from the eastern Mediterranean and central Europe. The LO-OOA factor had a very similar composition to the MO-OOA factor, but was more prevalent during westerly winds with air masses originating from the Atlantic Ocean, the western Mediterranean, and in high altitudes over France and Spain from mistral winds. The MSA-OOA factor contributed an average 12% to the PM_1 OA and was more dominant during the mistral winds. The HOA, representing observed primary organic aerosol only contributed 8% of the average PM_1 OA during the campaign.

Even though Lampedusa is one of the most remote sites in the Mediterranean, PM_1 concentrations (10 ± 5 μg m^{-3}) were comparable to those observed in coastal cities and sites closer to continental Europe. Cleaner conditions corresponded to higher wind speeds. Nucleation and growth of new aerosol particles was observed during periods of northwesterly winds. From a climatology analysis from 1999 until 2012, these periods were much more prevalent during the measurement campaign than during the preceding 13 years. These results support previous findings that highlight the importance of different large-scale synoptic conditions in determining the regional and local aerosol composition and oxidation and also suggest that a non-polluted surface atmosphere over the Mediterranean is rare.

1. Introduction

The Mediterranean Sea is a unique marine environment, surrounded by mountain ranges and high coastal human populations from Africa, Europe, and Asia, and the two largest deserts in the world; Sahara Desert to the south and Arabian Desert to the East. It presents a diverse and dynamic atmospheric composition and is projected to undergo significant changes in the contribution of freshwater (Sanchez-Gomez et al., 2009), sea surface temperature and precipitation (Mariotti et al., 2015) over the coming decades. The burning of fossil fuels, including shipping pollution, in southern Europe and in large Mediterranean cities, as well as natural sources of aerosol such as sea salt, forest fires and mineral dust provide a highly

complex and dynamic mixture of organic and inorganic aerosol and aerosol precursors in this region (Lelieveld et al., 2002). Elevated aerosol loadings over the Mediterranean basin have been attributed to the long-range transport of continental anthropogenic aerosols (Perrone et al., 2013; Sciare et al., 2003; Sciare et al., 2008) and mineral dust transported from Africa (Querol et al., 2009b; Koçak et al., 2007). Boundary layer observations in the eastern Mediterranean have shown significant influence of long-range transported continental pollution from southern and central Europe (Sciare et al., 2003). Furthermore, biomass burning aerosol has frequently been observed over the basin, in particular the dry season in summer when forest fires are more common (Bougiatioti et al., 2014; Minguillon et al., 2015; Pace et al., 2005). Long-ranged plumes from North American fires have also been observed at high altitudes (Formenti et al., 2002; Ortiz-Amezcua et al., 2014; Brocchi et al., 2018; Ancellet et al., 2016).

Previous long-term observations of the chemical composition of aerosol in the Mediterranean have shown that PM_{10} (particulate mass with aerodynamic diameter less than 10 µm) is composed of secondary ammonium sulphate, primary and secondary organic aerosol from fossil fuels or biogenic origins, with contributions from natural aerosols from the Sahara Desert and sea spray (Bove et al., 2016; Koulouri et al., 2008; Schembari et al., 2014; Calzolai et al., 2015). Mineral and sea salt contributions are significantly less in $PM_{2.5}$ particle fraction (Querol et al., 2009a). Coarse mode particles contribute to the direct radiative effect over the Mediterranean (Perrone and Bergamo, 2011; Meloni et al., 2006) and can also act as condensation sinks for pollutants (Pikridas et al., 2012). Smaller (sub-micron) aerosol particles, while also contributing efficiently to the total aerosol optical depth in this region (Formenti et al., 2018), can also act as efficient cloud condensation nuclei and therefore have influence on cloud formation, lifetime and precipitation (Haywood and Boucher, 2000). Understanding the impact of different natural and anthropogenic sources on the regional composition of the atmosphere is therefore important in our understanding of the influences they have on the climate over the Mediterranean basin and surrounding regions. It is also now widely recognised that aerosols contribute to adverse health effects in humans (World Health Organization, 2016).

Consideration of both the local and regional meteorology are needed to characterise the sources and aging of aerosols (Petit et al., 2017). The National Oceanic and Atmospheric Administration's (NOAA) Hybrid Single-Particle Lagrangian Integrated Trajectory model (HYSPLIT; Stein et al., 2015) and other trajectory models (e.g. FLEXPART; (Stohl et al., 2005)) have become a widely-used resources in atmospheric studies to compute the backwards or forwards trajectories of air masses at any point on Earth. They can be useful for identifying the possible origin of a particular episode associated with elevated concentrations of aerosols or

gases. Combined with in-situ measurements over longer time periods, they provide a more holistic approach in understanding the link between local or region meteorology and atmospheric composition (Schmale et al., 2013; Tadros et al., 2018; Zhou et al., 2016). This is particularly useful for remote sites where local emissions are insignificant or infrequent.

Investigation of the aerosol physical and chemical properties can also help distinguish their respective sources. Positive matrix factorisation (PMF; (Paatero, 1997; Paatero and Tapper, 1994)) has proved to be a useful statistical tool in identifying aerosol sources or aging processes of organics. The source apportionment of $PM_{2.5}$ and PM_{10} over the Mediterranean, from PMF method, has been investigated in recent works and showed a large spatial variability in source contributions (Becagli et al., 2012; 2017; Calzolai et al., 2015; Amato et al., 2016; Diapouli et al., 2017). The PMF approach was also used to study the aerosol source and aging processes by utilising the complex nature of organic aerosol in the Mediterranean (e.g. Hildebrandt et al., 2010, 2011; Bougiatioti et al., 2014; Minguillón et al., 2016; Arndt et al., 2017; Michoud et al., 2017). This approach has become increasingly feasible with the recent widespread implementation of instruments capable of providing real-time, high time-and mass-resolved non-refractory aerosol composition, such as aerosol mass spectrometers (Ulbrich et al., 2009). PMF models have shown to successfully resolve the bulk-composition of sub-micron organic aerosol into the contributions from various primary sources (e.g. biomass burning, fossil fuel burning, cooking aerosol), but can also reveal the contributions and characteristics of secondary (SOA) organic aerosol (Zhang et al., 2011). Factors with similar mass spectra are consistently observed, albeit with different contributions at measuring sites all around the world. The most commonly observed primary organic aerosol factors are hydrocarbon-like OA (HOA), usually from fossil fuel burning as well as biomass burning (BBOA) while SOA can be usually separated into at least two factors, with low-volatility oxygenated OA (LV-OOA) and Semi-Volatile-OOA (SV-OOA) as common examples (Zhang et al., 2011; Crippa et al., 2014). Other types of OOA have also been observed, such as "Marine-OOA" (Schmale et al., 2013), although these are more difficult to resolve given the shift towards more uniform OA composition with aging.

The Chemistry-Aerosol Mediterranean Experiment (ChArMEx) collaborative research program, and the Aerosol Direct Radiative Impact on the regional climate in the MEDiterranean region (ADRIMED) project within, were undertaken to investigate the chemistry and climate interactions within the Mediterranean (Mallet et al., 2016). From 11 June until 5 July 2013, numerous experimental setups were deployed across the western and central Mediterranean in what is called the "Special Observation Period - 1a" (SOP-1a), including intensive airborne measurements (Denjean et al., 2016). Two super-sites were set-up at Ersa (at the northern tip of Corsica Island, France) and at the Lampedusa Island (Italy), approximately 1000 km apart on a

north-to-south axis in order to characterise surface aerosol chemical, physical and optical properties (Mallet et al., 2016). Numerous secondary sites established along the Mediterranean coasts in Spain, Italy and Corsica beyond the SOP-1a have also provided valuable knowledge of the atmospheric composition in the western and central Mediterranean regions (Chrit et al., 2017; Chrit et al., 2018; Becagli et al., 2017).

In this paper, we present the first detailed characterisation of PM_1 in the central remote Mediterranean region, using measurements of size-resolved chemical composition on the island site of Lampedusa during the ChArMex/ADRIMED SOP-1a. We investigate the source apportionment of PM_1 by considering their chemical and microphysical properties along with ancillary PM_{10}, gaseous and meteorological data, air mass back trajectories as well as complimentary data collected at the Ersa site in Corsica.

2. Experimental

2.1 Sampling sites

Observations took place at the Roberto Sarao station on the island of Lampedusa (35°31'5''N, 12°37'51'' E, 20 m above sea level) from 11 June to 5 July 2013. Ancillary measurements for this study taken at Ersa at the northern tip of Cape Corsica (42°58'5'' N, 9°22'49'' E, 560 m above sea level), are also considered. The position of the stations is shown in Figure 1.

2.2 Instrumentation, measurements and data

Instruments at the Lampedusa super-site were housed in the PEGASUS (Portable Gas Field and Aerosol Sampling Unit) station, a portable observatory initiated by LISA, described in Mallet et al. (2016). Relevant to this study, a c-ToF-AMS (Aerodyne Inc., Billerica, USA), was used to measure the size-resolved composition of non-refractory particulate matter below 1 µm (NF-PM_1)(Drewnick et al., 2005). Data was collected with a 3-minute time resolution. The c-ToF-AMS was operated from a certified Total Suspended Particulate (TSP) sampling head (Rupprecht and Patashnick, Albany, NY, USA) followed by a cyclone impactor cutting off aerosol particles larger than 1 µm in aerodynamic diameter (using a flow rate of 16 lpm). A nafion drier was used, however the relative humidity at the inlet of the c-ToF-AMS was checked throughout the campaign and was always below 55%.

A particle-into-liquid sampler (Metrohm PILS; Orsini et al. (2003)) was installed on a TSP inlet

and collected samples approximately every hour. Denuders to remove acid/base gases were not used. Samples were analysed for major inorganic and organic anions (F^-, Cl^-, NO_3^-, SO_4^{2-}, PO_4^{3-}, $HCOO^-$, CH_3COO^-, $(COO^-)_2$) and cations (Na^+, NH_4^+, K^+, Ca^{2+}, Mg^{2+}) using Ion Chromatography (Metrohm, model 850 Professional IC) equipped with Metrosep A supp 7 pre-column and column for anions measurements and Metrosep C4-250 mm pre-column and column for cations measurements, and a 500 µL injection loop. The device was operated with a 1-hour time resolution.

A 13-stage rotating cascade impactor nanoMOUDI (Model 125B, Marple et al., 1991) was used to measure the size-segregated inorganic elemental composition. The nanoMoudi impactor, also operated from the TSP inlet, allows the separation of the particles in 13 size classes from 10 nm to 10 µm diameter with a backup stage. Each sample was collected for 3 days with a flow rate of 10 lpm to ensure enough material was collected on each impactor stage. 47 mm diameter PTPE filters (2 µm pore size) were used and coated with high quality vacuum grease (Dekati DS-515) to avoid bouncing. They were then analysed using X-ray fluorescence (PW-2404 spectrometer by PANalytical™) for the particulate elemental concentrations for elements from Na to Pb as described in Denjean et al. (2016)).

A Scanning Mobility Particle Sizer (SMPS) measured the mobility number size distribution of aerosols every 3 minutes from 14.6 to 661.2 nm diameter. The instrument is composed by an X-ray electrostatic classifier (TSI Inc., model 3080) and a differential Mobility Analyser (DMA; TSI Inc., model 3081), and a condensation particle counter (CPC; TSI Inc., model 3775) operated at 1.5/0.3 L min^{-1} aerosol/sheath flows. Data were corrected to take into account the particle electrical charging probabilities, the CPC counting efficiency, and diffusion losses. Each scan was recorded with a 5-minute time resolution. A drier was not used on the SMPS inlet and therefore the size distributions reported are for ambient conditions.

A GRIMM optical particle counter (OPC; GRIMM Inc., model 1.109) was used to measure the number size distribution over 31 size classes ranging from 0.26 µm up to 32 µm (nominal diameter range assuming the aerosol refractive index of latex spheres in the calibration protocol). The instrument was operated at a 6-second resolution and data were acquired as 3-minute averages.

The equivalent black carbon mass concentration (eBC) was determined by the measurement of light-attenuation at 880 nm performed by a spectral aethalometer (Magee Sci. model AE31) operated at a 2-minute time resolution and equipped with a TSP particle inlet. As the evaluation

of eBC is used as a qualitative tracer of pollution, the factory mass conversion factor of 16.6 m^2 g^{-1} was applied to the raw measurement of attenuation without further corrections.

The meteorological measurements (air pressure, temperature, relative humidity, wind direction and speed and precipitation) were collected by a Vaisala Milos 500 station with a sampling rate of 10 minutes. The wind sensor was installed on a 10-m meteorological tower, while the air temperature and humidity were measured at a height of 2 m.

2.3. Data analysis

2.3.1. Analysis of the cToF-AMS data

The cToF-AMS data set was processed using two different software analysis tools. The first makes use of the widely-used and standard Igor Pro package, Squirrel (version 1.57G). This software processes the raw data and analyzes the unit-mass resolution (UMR) output with a fragmentation table reported in Aiken et al. (2008). The second method uses a cumulative peak fitting analysis and residual analysis and allows the separation of multiple isobaric peaks not taken into account in the traditional analysis of unit mass resolution squirrel data treatment (Muller et al., 2011). Uncertainties in the major chemical species from the cToF-AMS are typically of the order of ±20% (Drewnick et al., 2005).

The ionization efficiency (IE) with respect to nitrate anions was calculated every 5-6 days using nebulised 350 nm mobility diameter ammonium nitrate particles (values varied between $1.42 * 10^{-7}$ and $1.53 * 10^{-7}$). The relative IE (RIE) of ammonium was slightly higher than the default value and was 4.3 based on the mass spectrum of ammonium nitrate data from IE calibrations. The RIE of sulfate was determined by comparing the theoretical and the measured concentration of a solution of ammonium nitrate and ammonium sulfate and was determined to be the default value of 1.2. For the organic fraction, the default value of 1.4 was used. For each of the major species, a composition dependent collection efficency was applied as proposed by Middlebrook et al., 2012 and was on average 0.549, very similar to the default value of 0.55.

The PM_1 sea salt concentration was estimated in the cTof-AMS by applying a scaling factor of 102 to the ion fragment (using the cumulative peak fitting analysis described in Muller et al., 2011) at 57.98 assigned to NaCl as proposed by Ovadnevaite et al., 2012. This scaling factor was determined by nebulising monodisperse 300 nm (mobility diameter) NaCl particles into the cToF-AMS and comparing the $NaCl^+$ signal to the total mass calculated using the number

concentration from a CPC-3010. This calibration was done after the campaign but with similar tuning conditions. The sea salt-SO_4^{2-} (ss-SO_4^{2-}) was calculated as 0.252 * 0.3 * [seasalt], where 0.252 is the mass ratio of SO_4^{2-} to Na^+ in sea salt and 0.3 is the mass ratio of Na^+ to sea salt (Ghahremaninezhad et al., 2016). Given these assumptions, the uncertainty in the seasalt concentrations are likely to be significantly higher than the typical 20%, although the total contribution of seasalt to the PM1 fraction was very small (0.30 µg m^{-3}; <4 %).

Unconstrained positive matrix factorisation was performed on both the unit-mass-resolution spectra of organic aerosol as well as the peak-fitted peaks identified as organics using PMF2 v2.08D. This method requires both a matrix for both the organic signals as well as the errors associated with the organics. For the peak-fitted signals, errors for each mass were estimated as

$$\Delta I/I = \sqrt{(\alpha^2 t + (\beta + 1)}$$

Where I is the ion signal, ΔI is the absolute uncertainty in the ion signal, α and β are constants (1.2 and 0.001, respectively) and t is the instrumental sampling time in seconds (Drewnick et al., 2009; Allan et al., 2003). For both UMR and peak-fitted inputs, up to 8 factors were investigated by altering the seeds from 0 to 50 in increments of 1 and the fpeaks from -1 to 1 in increments of 0.1. Where I is the ion signal, ΔI is the absolute uncertainty in the ion signal, α and β are constants (1.2 and 0.001, respectively) and t is the instrumental sampling time in seconds. For both UMR and peak-fitted inputs, up to 8 factors were investigated by altering the seeds from 0 to 50 in increments of 1 and the fpeaks from -1 to 1 in increments of 0.1. This approach is explained in Ulbrich et al. (2009).

2.3.2. Air mass back-trajectory calculation and cluster analysis

In order to determine potential source regions for aerosols measured at Lampedusa during the SOP-1a, a series of cluster analyses were performed on HYSPLIT air-mass back-trajectories as per the following. Weekly GDAS1-analysis (Global Data Assimilation System; 1° resolution) trajectory files were downloaded from the Air Resources Laboratory (ARL) of the National Oceanic and Atmospheric Administration (NOAA) archive. 144-hour air-mass backwards trajectories were then calculated every hour over the measurement period with ending point at Lampedusa (height of 45 m) using HYSPLIT (Stein et al., 2015) from within the R-package, SplitR. Cluster analyses were then performed on these calculated trajectories, using a trajectory clustering function within the R-package, OpenAir (Carslaw and Ropkins, 2012). Clustering was done using two different methods to calculate the similarity between different trajectories. The first uses the Euclidean distance between the latitude and longitude of each trajectory point (a

total of 144 in this case, representing each hour prior to the arrival at the receptor site). The second uses the similarity of the angles of each trajectory from the origin. These two methods are described in Sirois and Bottenheim (1995). For each clustering method, the number of clusters was altered from two up to ten. Six clusters identified using the Euclidean-distance method were selected, producing a realistic separation of the air-mass backwards trajectories and distinct and physically meaningful differences in aerosol composition and size. An additional clustering analysis was also performed over 3 and 6 hour intervals and using 96-hour backwards trajectories and yielded similar results.

3. Results and Discussion

3.1. Analysis of local and synoptic meteorology

The analysis of the hourly resolved 144-h air mass backwards trajectories provides an indication of the origin of the air masses sampled at Lampedusa during the field campaign. Six distinct clusters are identified (Figure 2). Cluster 1, "Eastern Mediterranean", is representative of air masses that circulate around the eastern-central Mediterranean basin before arriving at the Lampedusa site (average altitude of 400 m). Cluster 2, "Central Europe" is representative of air masses arriving from central Europe (average altitude of 800 m). Cluster 3, "Atlantic" is representative of more marine-like air masses that predominately originate over the Atlantic Ocean, pass over the Strait of Gibraltar between Spain and Morocco, and cross the western Mediterranean basin (average altitude of 500 m). Cluster 4, 263 "Western Europe", cluster 5, "Mistral (low)", and cluster 6, "Mistral (high)", all have similar angular trajectories, but are distinguishable by their different wind speeds and altitudes (although the Euclidian method of cluster analysis only considers differences in horizontal distances). The two "Mistral" clusters typically originate over the northern Atlantic Ocean, travel over France at a high altitude before descending over the western Mediterranean and travelling with relatively higher wind speeds towards Lampedusa. The altitude of "Mistral (high)" was, on average, higher than "Mistral (low)" (1400 m and 1000 m, respectively) and also coincided with higher wind speeds at Lampedusa (13 ms^{-1} and 9 ms^{-1}, respectively). In comparison, the trajectories of the "Western Europe" cluster spent much more time circulating at lower altitudes (700 m, on average) over the western Mediterranean basin and, to a certain extent, east of the Lampedusa site.

As a complement, the pressure, temperature, relative humidity, wind speed and direction time series recorded at the station are shown in Figure 3. Two main weather regimes are observed: the former characterized by intense (up to nearly 20 m s^{-1}) northwesterly winds, persisting for

several days (10-13 June and 22-30 June) and cool temperatures, whereas the latter associated with low-gradient anticyclonic conditions and light winds from the east or southeast, also favouring warmer temperatures (14-21 June and 1-3 July). Temperatures were relatively stable over the sampling period, fluctuating between approximately 18.5 °C and 28.2 °C. The relative humidity typically ranged from between 70% and 82% with very few and very brief episodes of drier air masses (relative humidity close to or below 50%). The wind speed and direction distributions during the campaign can be compared to the June-July climatology from 1999 to 2012 (Figure 4). During the sampling period of this study, the frequency of winds from the north-westerly sectors were nearly double the average when compared to normal conditions, approaching 40% with high winds speeds exceeding 10 m s^{-1} observed during more than 20% of the time.

Data of sea level pressure and 1000 mbar meridional wind component composite anomalies obtained from the National Center for Environmental Prediction (NCEP)/National Center for Atmospheric Research (NCAR) Reanalysis (Kalnay et al. 1996) indicate that this particular situation was induced by a "dipolar" pattern, characterized by positive pressure anomalies in the Western Mediterranean and negative ones in the eastern part of the basin (see Supplementary Figure S1). This produced a persisting, stronger than normal gradient over Southern Italy. As a consequence, surface dust episodes typically driven by strong south or southeasterly winds, associated to cyclonic systems moving along northern African coasts, were basically absent during the campaign.

3.2 Aerosol composition

The dry NR-PM_1 concentrations measured at Lampedusa by the cTof-AMS ranged from 1.9 to 33.4 µg m^{-3}, with a mean of 10.2 µg m^{-3} over the sampling period. Sulphate contributed the most to the measured NR-PM_1 mass (41% ± 9% on average) followed by significant contributions from organics (31% ± 8%) and ammonium (17% ± 3%). The eBC, nitrate and sea salt (scaled from the NaCl component of m/z 58) contributed 6% (±4%), 1% (±0.4%) and 3% (±2%), respectively. Figure 5 shows the total PM_1 concentration (calculated as the sum of the individually measured species), with contribution from each of the species, as well as the calculated PM_1 mass concentration from the SMPS (assuming an average density based on the composition data). There was reasonable agreement (slope = 0.62; R^2 = 0.67) between the PM_1 mass concentration calculated from composition measurements and the SMPS, with discrepancy observed during periods of high sulphate concentrations from the eastern Mediterranean. This could be due to a combination of a broader accumulation mode exceeding the upper size limits of the cToF-AMS inlet, differences in sampling line relative humidity, or

unaccounted for variations in the collection efficiency. This figure also contains an indication of the air mass origin over the sampling period.

During most of the campaign there was a reasonable agreement (slope = 1; R^2 = 0.6) between the PM_1 SO_4^{2-} (c-ToF-AMS) and the TSP SO_4^{2-} (PILS) concentration, with the exception of periods of high sea salt concentrations when the TSP SO_4^{2-} were significantly higher (slope = 0.5; R^2 = 0.2 for TSP Cl- concentrations > 10 µg m^{-3}; see Supplementary Figure S2). Supporting measurements of the size-segregated composition from the cascade impactor corroborate this, indicating a higher contribution of elemental sulphur in the coarse mode during periods of higher sea salt (Supplementary Figure S3). These periods corresponded to the "Mistral" air masses, characterised by higher wind speeds and indicated the role of coarse sea salt particles in acting as a condensation sink for sulphate species. If these events are frequent, this could have important implications for the radiative properties of these aerosols by altering the scattering properties and, potentially cloud condensation nuclei concentrations and composition.

Figure 6 shows the organic mass, split according to different OA factors from the PMF of the OA peaks. From the unconstrained PMF of the UMR and peak-fitted organic mass spectra, the most meaningful solution was found from a 4-factor solution of the UMR analysis (see Supplementary Figures S4 and S5 for the mass reconstruction and time series' residuals). This has resulted in one factor resembling to a primary organic aerosol and three oxygenated organic aerosol (OOA) factors. Herein we label these factors HOA (hydrocarbon-like OA), MO-OOA (more oxidised OOA), LO-OOA (less oxidised OOA) and MSA-OOA (methanesulfonic acid-related OOA).

These factors were compared with ambient organic mass spectra listed in the AMS Spectral Database (Ulbrich et al., 2009). The spectra for the OOA factors (see Figure 7) were strongly correlated with each other (R > 0.97) and all three were similar to a "continental" OOA factor observed in a ship campaign in the Artic (Chang et al., 2011), as well as a low-volatility OOA factor identified in Paris (Crippa et al., 2013). Despite the similarities in their mass spectra, they exhibited different diurnal trends (Figure 7) and time series that were associated with different wind directions and air masses and were therefore not recombined into a single OOA factor.

The MO-OOA factor was the most dominant factor during the field campaign (~53% of the total OA mass) and was typical of low-volatility/highly oxidized OOA observed in many other studies, in the Mediterranean, with high contributions of m/z 44 (f_{44} = 0.31) (e.g. (Hildebrandt et al., 2010; Hildebrandt et al., 2011). This factor was the most prominent during air masses from the Eastern Mediterranean, central Europe and Atlantic (contributing to 71%, 58% and 55% to OA,

respectively) and was strongly correlated with ammonium sulphate (R^2 = 0.68) over the whole campaign. It also had a distinct diurnal trend, with concentrations increasing during daylight hours, indicative of photochemical processing. The LO-OOA factor was slightly less oxygenated (f_{44} = 0.26) and exhibited a different time series (R^2 = 0.04), related to different air masses, than the MO-OOA. The less oxygenated OOA factor has also been associated with semi-volatile species and is often labelled as SV-OOA (Jimenez et al., 2009). Despite a distinct diurnal profile similar to previously reported SV-OOA factors (with a peak in the early morning), we refrain from labelling our LO-OOA this way because the mass spectrum was generally much more oxygenated and contained less f_{43} than typically reported SV-OOA (see Figure 9).

The MSA-OOA factor contributed approximately 12% of the total OA during the campaign and is likely related to the biogenic emission and processing of dimethyl sulfide (DMS) from phytoplankton in the Mediterranean. This factor was also highly oxygenated (f_{44} = 0.20), but contains key peaks related to the fragmentation of MSA from the electron impact of the cToF-AMS. The most prominent of these peaks were m/z 96 ($CH_4SO_3^+$), 79 ($CH_3SO_2^+$), 78 ($CH_2SO_2^+$), 65 (HSO_2^+) and 45 (CHS^+). A similar factor was observed at Bird Island in the south Atlantic Ocean (Schmale et al., 2015), albeit without the contribution of significant m/z 44, suggesting a more aged or mixed aerosol during this campaign. A distinct diurnal pattern for the MSA-OOA was not observed.

While the MO-OOA, LO-OOA and MSA-OOA factors represent secondary organic aerosol and were the most dominant contribution of OA during the campaign (92% on average), a primary organic aerosol factor was observed and identified here as hydrocarbon-like OA (HOA). The mass spectrum of the HOA factor was characteristic of spectra observed in other studies, with prominent peaks at m/z 95, 91, 83, 81, 71, 69, 57, 55, 43 and 41. Although HOA is typically associated with emissions from incomplete combustion (Zhang et al., 2005), it was not well correlated with other expected tracers such as eBC, CO and NOx. This HOA was typically associated with south-westerly winds of low speed (<5 m s^{-1}; see Figure 10) and peaked at approximately 6 am local time each morning. The poor correlation between the HOA factor and eBC could have been due to a variety of local sources with different HOA and eBC emission factors, a mixing of the PMF factor with some small peaks not associated with combustion processes or from regional HOA that has undergone some transport without significant oxidation. The signal fraction of each m/z of the mass spectrum of the HOA factor however had strong correlations (0.69 < R < 0.89) with numerous hydrocarbon-like organic aerosol (HOA) factors from other studies (Hersey et al., 2011; Ulbrich et al., 2009; Ng et al., 2011; Lanz et al., 2007; Zhang et al., 2005).

388 3.3 Comparison with other observations around the Mediterranean

389 There are many factors that could influence the composition, the concentration, and oxidation
390 level of different aerosol species over the Mediterranean. These include different aerosol
391 sources which can follow different seasonal or yearly trends (e.g. biogenic emissions) as well as
392 the existing aerosol load and the meteorological conditions that drive transport, dilution and
393 aging processes. The majority of previous studies of detailed PM_1 aerosol composition have
394 been taken at coastal sites around the Mediterranean (Mohr et al., 2012; Minguillón et al.,
395 2016; Minguillón et al., 2015; Haddad et al., 2013; Bozzetti et al., 2017) which could be
396 expected to observe higher concentrations than at Lampedusa due to proximity to sources (e.g.
397 traffic, fossil fuel use, heating, biomass burning, industrial activities). Aside from Lampedusa and
398 the observations presented in this study, measurements at Finokalia and Cape Corsica could be
399 considered the most remote sites where these measurements have been taken. Similar to the
400 comparison of NR-PM1 measurements from Europe, North America and east Asia made by
401 Zhang et al., 2007, Figure 8 summarises the recent observations of NR-PM_1 composition from
402 measurements in and around the Mediterranean basin (see Supplementary Tables S1 and S2 for
403 more details that are displayed in Figure 8).

404 The PM_1 mass loading observed at Lampedusa is comparable to most of these other studies
405 performed at both remote marine sites and coastal sites in the Mediterranean . With the
406 exception of sites in the eastern Mediterranean, OA was the dominant NR-PM_1 constituent and
407 summertime OA was generally considered mostly secondary, comprised of SV-OOA and LV-OOA
408 with small contributions of HOA. For remote sites, the results are consistent with a
409 predominance of OA in PM_1 fraction in summer. PMF analysis of Q-AMS measurements at the
410 Finokalia remote site in the eastern Mediterranean in the summer of 2008 showed two OOA
411 factors and a distinct lack of HOA (Hildebrandt et al., 2010). A more recent study during the late
412 2012 summer at Finokalia observed periods influenced by biomass burning, but otherwise also
413 observed mostly oxygenated organic aerosol (Bougiatioti et al., 2014). Measurements
414 undertaken in the western Mediterranean at Cape Corse from 11 June until 6 August 2013,
415 encompassed the sampling period of this study. For the period from 15 July until 5 August, PMF
416 analysis showed 55%, 27% and 13% contributions of organic matter, sulphate and ammonium
417 to non-refractory PM_1 (Michoud et al., 2017). Secondary oxygenated VOCs dominated the VOC
418 spectrum during the campaign and were very well correlated with submicron organic aerosol.
419 PMF analysis on the OA revealed a 3-factor solution where SV-OOA and LV-OOA were
420 dominant, contributing by 44% and 53%, respectively, with a 4% HOA contribution. From the
421 same measurements but reported over the extended period from 11 June 11 until 5 August 5,
422 there was a higher LV-OOA contribution (62%)(Arndt et al., 2017) which is in agreement with

our observations of MO-OOA at Lampedusa. The OA was mostly portioned into MO-OOA and LO-OOA (81%), indicative of well-aged or oxidised secondary organic aerosol from long-range transport of pollutants.

Figure 9 displays the behavior of the f_{44} and f_{43} fragments obtained during the field campaign. f_{44}, a proxy for OA oxidation (Jimenez et al., 2009), is calculated as the ratio of the mass at m/z 44 (mostly CO_2^+) to the total OA, while f_{43}, equal to the ratio of m/z 43 (mostly $C_2H_3O^+$) to the total OA, typically represents less aged OA. f_{44} was ~0.26 for the majority of the sampling period (Q1; 0.25, Q3: 0.27), while f_{43} was 0.036 (Q1: 0.028, Q3: 0.041). The campaign values are compared to values from the spectra for the four PMF factors and those observed in other field campaigns in the remote Mediterranean. The dotted lines (the so-called "Ng triangle"), encapsulate the f_{44} and f_{43} values of atmospheric OA from a vast number of studies (Ng et al., 2010), with the most aged OA in the top left corner and the most fresh in the bottom right. The high f_{44} values and the dominance of the highly oxygenated MO-OOA and LO-OOA factors show that the organic aerosol was extremely aged compared to other measurements.

3.4 Links to meteorology

The contribution of the major submicron chemical species and OA sources is further explained in the following by linking the measured and apportioned concentrations to the local meteorology (i.e., wind speed and wind direction) and to the air mass back trajectories to account for the long-range transport of aerosol as well as more distant sources. The bivariate polar plots of these PM_1 species and f_{44} as a function of wind speed and direction are shown in Figure 10.

Considering that the sampling site on Lampedusa is on the north east tip of the island, it is evident that the SO_4^{2-} and NH_4^+ were likely a result of north-easterly marine air masses, in agreement with previous results (e.g., Bove et al., 2016). Sea salt concentrations were highest during high north-westerly wind speeds. Higher concentrations of NO_3^-, HOA and some of the periods with elevated eBC concentrations were observed during low speed south-westerly winds, likely a result of the human settlements and activity on the island of Lampedusa (population of ~6000 located to the south west of the sampling site). Besides, the polar plot for eBC showed a patchier pattern, indicative of more local or point sources and the elevated signals were likely due to air masses passing over ship plumes. Although the mass spectra for the LO-OOA and MO-OOA factors were very similar, their bivariate polar plots indicate different sources or photochemical processes. The MO-OOA was more prominent during north-easterly winds, indicating the most aged organics were influenced by air masses from the eastern Mediterranean, either from long-ranged transport or from circulation of closer pollution

sources, while the LO-OOA was more dominant during northwesterly wind directions and air masses from over the western Mediterranean. Figure 11 shows the average contribution of each species during different air mass periods (see Supplementary Table S2 for the mean concentrations and standard deviations).

The highest concentrations of PM_1 were observed during "Eastern Mediterranean" and "Central Europe" air mass periods, when significant lifetime over the lower altitude marine environment and/or higher SO_2 emissions allowed the conversion and condensation of sulphate. These aged aerosols are corroborated by the high number concentrations within the accumulation mode during these periods relative to other periods, measured by the SMPS as well as the size-resolved sulphate composition, as discussed in the next section. In contrast to the "Eastern Mediterranean" and "Central Europe" air masses, sulphate concentrations were relatively low during the two "Mistral" air masses. This behavior has been found also in PM_{10}, with elevated values of sea salt aerosol and low non-sea salt sulphate during Mistral events (Becagli et al., 2017). The organic mass concentration was relatively uniform across the periods of different air mass origins, with the exception of the high Mistral winds which yielded OA concentrations approximately half the rest of the campaign and a higher contribution of MSA-OOA in comparison with other periods. The higher contribution of MO-OOA compared with LO-OOA from eastern air masses, and vice-versa during western air masses, could be indicative of different OA sources prior to oxidation or due to different photochemical aging between the two directions.

3.5 Aerosol size distributions

There are distinctions between the measured PM_1 size distributions during periods of different air mass origins (Figure 12). It should be noted that these size distributions are under ambient conditions without an inlet drier which could shift the size distribution to larger sizes if water is present. The ambient relative humidity for each air mass back trajectory cluster was: Eastern Mediterranean (53%), Central Europe (61%), Atlantic (74%), Western Mediterranean (70%), Mistral (low) (67%) and Mistral (high) (74%). Although the higher temperature inside the PEGASUS mobile laboratory could lower the relative humidity at the sampling point of the SMPS with respect to the ambient relative humidity, this was not measured or logged during the campaign.

Consistent with the higher concentrations of sulphate and ammonium species, the "Eastern Mediterranean" and "Central Europe" had the most pronounced accumulation modes with respect to those from other clusters due to the presence of accumulation mode sulphate (see Supplementary Figure S6 for the size-resolved chemical composition). In contrast, the "Mistral

(high)" air masses had very few particles in the accumulation mode and were mostly dominated by nucleation (> 14 nm observations only) and Aitken mode particles, in terms of number. There was only one period of "Mistral (high)" air masses, spanning 38 hours between 09:00 on 24 June until 23:00 on 25 June.

The most pronounced new particle formation (NPF) events and subsequent growth were observed during the two "Mistral" air masses, particularly between 25 and 27 June. Very high number concentrations in the nucleation mode were also observed in very brief periods during the Atlantic and, to an extent, the "Western Europe" air masses. There was a no trend (R^2 = 0.03) over the whole campaign between the ratio of the particle number concentration between 14 -25 nm and 14 -600 nm and the fraction of $CH_3SO_2^+$ (a fragment of MSA, measured by the cToF-AMS) to total PM_1 organics (see Supplementary Figure S7. There was a weak positive trend during periods of the Mistral (high) air mass (R^2 = 0.39). No trends were observed between the ratio of sub-25 nm and sub-600 nm particle number concentrations and the occurrence of other cToF-AMS fragments such as amines that could be linked with biogenic gas-to-particle conversion. Furthermore, there was a weak negative trend between the ratio of sub-25 nm and sub-600 nm particle number concentrations and the calculated f_{44} (R^2 = 0.12). Without instrumentation to measure the concentration of clusters and smaller aerosols (<14 nm) in conjunction with organic vapours over a longer time period, it is difficult to isolate and conclude the origin of these nucleation particles in a general sense and we will limit our analysis to the most pronounced event during the campaign. Figure 13 shows the size distribution over this period as well as SO_2, eBC and $CH_3SO_2^+$, as well as the back trajectory ending at 04:00 UTC on 25 June at Lampedusa. This NPF event occurred during the night and therefore in the absence of photochemistry. There was no discernible increase in eBC or SO_2 during these events and the 3-day cascade impactor sample from 25 until 28 June was characterized by the lowest concentrations of vanadium and nickel (released from heavy oil combustion events due to ship emissions) of the whole campaign. The air mass backwards trajectory during this event was characteristic of the "Mistral (high)" cluster. These are high altitude air masses descended over the Atlantic Ocean before having undergone a hydraulic jump over the southern France region and then a rapid descent over the western Mediterranean basin at high speed before arriving at the Lampedusa site. It is interesting to note that these air masses were anomalous for the typical June/July period at Lampedusa. Although the detected mass of $CH_3SO_2^+$ is likely due to the condensation of MSA on accumulation mode particles, and considering that the cTof-AMS collection efficiency below ~100 nm is poor, the increasing concentration of $CH_3SO_2^+$ did coincide with the nucleation events during this period, suggesting a possible nucleation and condensation of marine biogenic vapours. Different studies indicate that NPF events may be

triggered by atmospheric mixing processes (Kulmala et al., 2004; Hellmuth, 2006; Lauros et al., 2007; Lauros et al., 2011) due to different phenomena like the enhancement of turbulence in elevated layers (Wehner et al., 2010), the break-up of the nocturnal inversion (Stratmann et al., 2003), or the turbulence associated with the nocturnal low-level jet (Siebert et al., 2007). Night-time NPF events have also been observed in the Eastern Mediterranean (Kalivitis et al., 2002).

Furthermore, the intrusion of descending mid-tropospheric air masses in the boundary layer (Pace et al., 2015) has been linked to the occurrence of NPF events and would be consistent with the absence of high concentrations of BC, SO_2, vanadium and nickel which could be expected from ship emissions (Healy et al., 2009; Isakson et al., 2001) in the boundary layer over the Mediterranean. Pace et al. (2006) have shown that clean marine aerosol conditions are rare at Lampedusa and generally associated with north-westerly progressively descending trajectories, in agreement with the findings of this study. The relative absence of pre-existing particles acting as a condensation sink favors NPF events as observed during the field campaign.

3.6 Accumulation of sulphates across the Mediterranean

In order to investigate the aging of aerosols across the north-south trajectory of European continental air masses, we compare the average NR-PM_1 composition measurements at Lampedusa to the concurrent measurements conducted at the Ersa site during summer 2013 (Michoud et al., 2016; Arndt et al., 2017). This is shown in Table 1.

On average, the PM_1 non-refractory organic mass concentrations at both sites were similar with ~3 µg m^{-3}. NO_3^- concentrations were relatively small at both sites, but higher at Ersa (0.28 µg m^{-3}) than at Lampedusa (0.09 µg m^{-3}). Sulphate concentrations were a factor of 3.2 times higher at Lampedusa (4.5 µg m^{-3}) than at Ersa (1.4 µg m^{-3}) while the ammonium concentrations were a factor of 2.7.

To investigate the possible accumulation of ammonium sulphate during the transport of air masses from Europe, the hourly air-mass back trajectories from Lampedusa were filtered so that only those that passed within ±1° latitude and longitude and within ±200 m altitude of the station height of Ersa (550 m) were selected. These thresholds were chosen arbitrarily since there is no clear distinction in horizontal or vertical distance from the site that would necessarily constitute a representative air mass. This resulted in a total of 192 hourly observations at the Ersa site over 32 unique air mass backward trajectory runs (see Figure 14).

These trajectories were grouped mainly into the "Central Europe" cluster (n = 12). The median trajectory duration between the Ersa and Lampedusa sites was 53 hours, with a minimum of 33

hours and a maximum of 144 hours (corresponding to the total duration of the HYSPLIT model runs in this case). Those air masses grouped in the "Eastern Mediterranean" cluster had the longest duration time between the sites of 127 hours (while coincident with the Ersa site, these air masses still spent a significant amount of time over the eastern Mediterranean), followed by "Central Europe" (83 hours), "Western Europe" (45 hours) and then the "Mistral (low)" (38 hours). In general, between the two sites, there was a 40% enhancement in the organic mass concentration, but an increase in sulphate and ammonium by a factor of 6 and 4, respectively (Table 1).

The accumulation of $(NH_4)_2SO_4$ between Ersa and Lampedusa appeared to be dependent on the travel time of the air mass, however different relationships were observed during different air mass clusters. The total sulphate concentration at Lampedusa minus the total sulphate concentration at Ersa for the same air mass and accounting for the travel time as a function of the travel time is shown in Figure 15.

There was a good positive correlation between the difference in sulphate concentrations between the two sites and the travel time for the "Central Europe" and "Eastern Mediterranean" air masses, while weak positive correlations were observed for the "Western Europe" and "Mistral (low)" clusters. It should be pointed out that the travel time was more than 110 hours for the "Eastern Mediterranean" air masses, while it was only between 33 and 58 hours for the other three air mass clusters. It is expected that the accumulation of sulphate would increase as the total travel time increases due to the opportunity for SO_2 conversion or from the addition of sulphate from separate air masses which are not accounted for in the HYSPLIT model. Although this relationship is somewhat demonstrated here, there are other factors that would influence the SO_4^{2-} accumulation. The sulphate concentrations presented here are measured by an ACSM and cToF-AMS at the Ersa and Lampedusa sites, respectively. Both of these instruments have a 100% inlet efficiency between ~100 nm and 800 nm. The conversion of SO_2 to SO_4^{2-} via nucleation and condensation is dependent on the pre-existing aerosol size distribution and condensation sink. Therefore, the use of PM_1 composition can be misleading if the sulphate is condensing on coarse particles. This is demonstrated in Supplementary Figure S2 that shows the size-resolved mass distribution of sulphur and sodium collected every 3 days on multi-stage cascade impactor filters; the relative contribution of sulphur in the PM_1 is higher than that of PM_{10} in the absence of sodium (a tracer for sea salt). Furthermore, the concentrations of SO_4^{2-} measured by the PILS in the PM_{10} fraction and cToF-AMS in the PM_1 are approximately equal with low sea salt concentrations ($Na+ < 2\ \mu gm^{-3}$), but are nearly a factor of two higher with the PILS for higher sea salt concentrations (Supplementary Figure S3). Furthermore, the emission of SO_2, typically from ships in the

Mediterranean, is not necessarily constant over time and is likely not uniformly spread over the basin and within the vertical column (e.g., Becagli et al. (2017)). This could possibly explain the discrepancy between the "accumulation rate" of sulphate between the Eastern Mediterranean and Central European air mass origins. Moreover, the sample size for this analysis is relatively small and potentially not representative of the general accumulation of SO_4^{2-} but nonetheless they highlight the magnitude of accumulation under different air mass trajectories.

4. Concluding remarks

The measurements carried out at Lampedusa during the ChArMEx/ADRIMED SOP-1a field campaign has provided a unique insight into the surface layer aerosols in the remote Central Mediterranean. Air masses were influenced by transport from the eastern Mediterranean, central Europe, the western Europe, the Atlantic Ocean as well as western Europe. Air mass clustering has been performed to explain observed differences in the aerosol composition and size at Lampedusa.

Hourly PM_1 mass ranged from 1.9 to 33.4 µg m^{-3}, with an average of 10.2 µg m^{-3}. It was composed on average of 41% ± 9% sulphate, 31% ± 8% organics, 17% ± 3% ammonium, 6% ±4% black carbon, 1% ± 0.4% nitrate and 3% ± 2% sea salt. OA was highly oxidized (f_{44} ~0.26), and was apportioned to more oxidised oxygenated OA factor (MO-OOA, 53%), less oxidised OOA factor (LO-OOA, 28%), methanesulfonic acid OOA (MSA-OOA, 12%) and to hydrogen-like OA (HOA, 8%). The highest PM_1 mass loadings were observed for air masses from the Eastern Mediterranean and central Europe, mostly due to the accumulation of ammonium and sulphate. Ancillary data from a remote site at the northern point of Cape Corsica in the Western Mediterranean showed increases of SO_4^{2-} concentrations between 2 and 12 µg m^{-3} when both sites (Corsica and Lampedusa) were connected. Apart from the dominance of ammonium sulphate on the PM_1 composition, the mass concentration and sources of OA have shown to be comparable to previous observations at European coastal and remote sites in the Mediterranean. The most pristine air masses, in terms of PM_1, were observed during periods with north-westerly winds which originated from the western Mediterranean or at high altitudes over the western European continent. Several nucleation and growth events, as well as large sea salt concentrations were observed during these pristine periods. The largest concentrations of PM_1 were observed from air masses from central Europe and those that had circulated over the eastern Mediterranean. In contrast to previous measurements of column-integrated aerosol optical properties (Pace et al., 2006; Meloni et al., 2006), we did not observe the presence of dust or biomass burning in the PM_1 range at the surface.

Our results also indicate a clear dichotomy of PM_1 aerosol composition from different source regions. Air masses from central Europe were characterised by a higher organic fraction than those from the eastern Mediterranean, which were enriched in sulphates. This difference could have potential implications on the optical properties and particularly the cloud condensation nuclei capabilities of those air masses. The relative occurrence of easterly air masses is not evident in the climatological wind roses, nor in a previous study by Pace et al. (2006) that took a climatological approach of the air mass back trajectories arriving at Lampedusa from 2001 - 2003. Nonetheless, a re-evaluation of the relative importance and occurrence of different air masses and aerosol properties should be undertaken.

Data availability. Open-access to the data used for this publication is provided to registered users following the data and publication policy of the ChArMEx program (http://mistrals.sedoo.fr/ChArMEx/ Data-Policy/ChArMEx_DataPolicy.pdf). Additional code used in the analysis of data can be obtained upon request from the corresponding or first author. Weekly GDAS1-analysis (Global Data Assimilation System; 1° resolution) trajectory files were downloaded from the Air Resources Laboratory (ARL) of the National Oceanic and Atmospheric Administration (NOAA) archive (ftp://arlftp.arlhq.noaa.gov/archives/gdas1/). 144-hour air-mass backwards trajectories were calculated using the R-package, SplitR (https://github.com/rich-iannone/SplitR). Cluster analyses were performed on these calculated trajectories, using the R-package, OpenAir (Carslaw and Ropkins, 2012); https://github.com/cran/openair). Spectra used for comparison of PMF OA factors from those observed in other studies can be found at http://cires.colorado.edu/jimenez-group/AMSsd/

Author contributions. PF, BD, KD, JFD, AGdS designed the experiment in Lampedusa, JS designed the experiment in Ersa, with contributions of co-workers. BD, AM, MCB, FC, GP, KD, CDB, JFD, MM, DM, JS, PZ, AGdS and PF performed the experiments. MDM, BD, AM, GP, KD, JS and PF analysed data and all authors contributed to data interpretation. MDM, BD, GP, KD and PF wrote the manuscript with contributions and/or comments from all co-authors.

Competing interests. The authors declare that they have no conflict of interest.

Special issue statement. This article is part of the special issue of the Chemistry and Aeosols Mediterranean Experiment (ChArMEx) (ACP/AMT inter-journal SI)". It is not associated with a conference.

Acknowledgements. This work is part of the ChArMEx project supported by CNRS-INSU, ADEME, Météo-France and CEA in the framework of the multidisciplinary program MISTRALS (Mediterranean Integrated Studies aT Regional And Local Scales; http://mistrals-home.org/). It

has also been supported by the French National Research Agency (ANR) through the ADRIMED program (contract ANR-11-BS56-0006). Measurements at Lampedusa were also supported by the Italian Ministry for University and Research through the NextData and RITMARE Projects. The AERIS national data infrastructure is acknowledged for maintaining the ChArMex database. Observations took place at the Roberto Sarao station (http://www.lampedusa.enea.it/).

References

Aiken, A. C., Decarlo, P. F., Kroll, J. H., Worsnop, D. R., Huffman, J. A., Docherty, K. S., Ulbrich, I. M., Mohr, C., Kimmel, J. R., and Sueper, D.: O/C and OM/OC ratios of primary, secondary, and ambient organic aerosols with high-resolution time-of-flight aerosol mass spectrometry, Environmental Science & Technology, 42, 4478-4485, 2008.

Allan, J. D., Jimenez, J. L., Williams, P. I., Alfarra, M. R., Bower, K. N., Jayne, J. T., Coe, H., and Worsnop, D. R.: Quantitative sampling using an Aerodyne aerosol mass spectrometer 1. Techniques of data interpretation and error analysis, Journal of Geophysical Research: Atmospheres, 108, 2003.

Ancellet, G., Pelon, J., Totems, J., Chazette, P., Bazureau, A., Sicard, M., Di Iorio, T., Dulac, F., and Mallet, M.: Long-range transport and mixing of aerosol sources during the 2013 North American biomass burning episode: analysis of multiple lidar observations in the western Mediterranean basin, Atmospheric Chemistry and Physics, 16, 4725-4742, 2016.

Arndt, J., Sciare, J., Mallet, M., Roberts, G. C., Marchand, N., Sartelet, K., Sellegri, K., Dulac, F., Healy, R. M., and Wenger, J. C.: Sources and mixing state of summertime background aerosol in the north-western Mediterranean basin, Atmospheric Chemistry and Physics, 17, 6975-7001, 2017.

Becagli, S., Sferlazzo, D. M., Pace, G., di Sarra, A., Bommarito, C., Calzolai, G., Ghedini, C., Lucarelli, F., Meloni, D., Monteleone, F., Severi, M., Traversi, R., and Udisti, R.: Evidence for heavy fuel oil combustion aerosols from chemical analyses at the island of Lampedusa: a possible large role of ships emissions in the Mediterranean, Atmos. Chem. Phys., 12, 3479–3492, 2012.

Becagli, S., Anello, F., Bommarito, C., Cassola, F., Calzolai, G., Di Iorio, T., di Sarra, A., Gómez-Amo, J.-L., Lucarelli, F., Marconi, M., Meloni, D., Monteleone, F., Nava, S., Pace, G., Severi, M., Sferlazzo, D.M., Traversi, R., and Udisti, R.: Constraining the ship contribution to the aerosol of the central Mediterranean, Atmospheric Chemistry and Physics, 17, 2067-2084, 2017.

Bougiatioti, A., Stavroulas, I., Kostenidou, E., Zarmpas, P., Theodosi, C., Kouvarakis, G., Canonaco, F., Prévôt, A., Nenes, A., and Pandis, S.: Processing of biomass-burning aerosol in the eastern Mediterranean during summertime, Atmospheric Chemistry and Physics, 14, 4793-4807, 2014.

Bove, M., Brotto, P., Calzolai, G., Cassola, F., Cavalli, F., Fermo, P., Hjorth, J., Massabò, D., Nava, S., and Piazzalunga, A.: PM10 source apportionment applying PMF and chemical tracer analysis to ship-borne measurements in the Western Mediterranean, Atmospheric Environment, 125, 140-151, 2016.

Bozzetti, C., El Haddad, I., Salameh, D., Daellenbach, K. R., Fermo, P., Gonzalez, R., Minguillón, M. C., Iinuma, Y., Poulain, L., and Elser, M.: Organic aerosol source apportionment by offline-AMS over a full year in Marseille, Atmospheric Chemistry and Physics, 17, 8247-8268, 2017.

Brocchi, V., Krysztofiak, G., Catoire, V., Guth, J., Marécal, V., Zbinden, R., Amraoui, L., Dulac, F., and Ricaud, P.: Intercontinental transport of biomass burning pollutants over the Mediterranean Basin during the summer 2014 ChArMEx-GLAM airborne campaign, Atmospheric Chemistry and Physics, 18,

6887-6906, 2018.

Calzolai, G., Nava, S., Lucarelli, F., Chiari, M., Giannoni, M., Becagli, S., Traversi, R., Marconi, M., Frosini, D., Severi, M., Udisti, R., di Sarra, A., Pace, G., Meloni, D., Bommarito, C., Monteleone, F., Anello, F., and Sferlazzo, D. M.: Characterization of PM10 sources in the central Mediterranean, Atmos. Chem. Phys., 15, 13939–13955, 2015.

Carslaw, D. C., and Ropkins, K.: Openair—an R package for air quality data analysis, Environmental Modelling & Software, 27, 52-61, 2012.

Chang, R.-W., Leck, C., Graus, M., Müller, M., Paatero, J., Burkhart, J. F., Stohl, A., Orr, L., Hayden, K., Li, S.-M., Hansel, A., Tjernström, M., Leaitch, W. R., and Abbatt, J. P. D.: Aerosol composition and sources in the central Arctic Ocean during ASCOS, Atmos. Chem. Phys., 11, 10619-10636, 2011.

Chrit, M., Sartelet, K., Sciare, J., Pey, J., Marchand, N., Couvidat, F., Sellegri, K., and Beekmann, M.: Modelling organic aerosol concentrations and properties during ChArMEx summer campaigns of 2012 and 2013 in the western Mediterranean region, Atmospheric Chemistry and Physics, 17, 12509-12531, 2017.

Chrit, M., Sartelet, K., Sciare, J., Pey, J., Nicolas, J. B., Marchand, N., Freney, E., Sellegri, K., Beekmann, M., and Dulac, F.: Aerosol sources in the western Mediterranean during summertime: A model-based approach, Atmos. Chem. Phys. Discuss., https://doi/. org/10.5194/acp-2017-915, in review, 2018.

Crippa, M., DeCarlo, P., Slowik, J., Mohr, C., Heringa, M., Chirico, R., Poulain, L., Freutel, F., Sciare, J., and Cozic, J.: Wintertime aerosol chemical composition and source apportionment of the organic fraction in the metropolitan area of Paris, Atmospheric Chemistry and Physics, 13, 961-981, 2013.

Crippa, M., Canonaco, F., Lanz, V., Äijälä, M., Allan, J., Carbone, S., Capes, G., Ceburnis, D., Dall'Osto, M., and Day, D.: Organic aerosol components derived from 25 AMS data sets across Europe using a consistent ME-2 based source apportionment approach, Atmospheric chemistry and physics, 14, 6159-6176, 2014.

Denjean, C., Cassola, F., Mazzino, A., Triquet, S., Chevaillier, S., Grand, N., Bourrianne, T., Momboisse, G., Sellegri, K., and Schwarzenbock, A.: Size distribution and optical properties of mineral dust aerosols transported in the western Mediterranean, Atmospheric Chemistry and Physics, 16, 1081-1104, 2016.

Drewnick, F., Hings, S. S., DeCarlo, P., Jayne, J. T., Gonin, M., Fuhrer, K., Weimer, S., Jimenez, J. L., Demerjian, K. L., and Borrmann, S.: A new time-of-flight aerosol mass spectrometer (TOF-AMS)—Instrument description and first field deployment, Aerosol Science and Technology, 39, 637-658, 2005.

Drewnick, F., Hings, S., Alfarra, M., Prevot, A., and Borrmann, S.: Aerosol quantification with the Aerodyne Aerosol Mass Spectrometer: detection limits and ionizer background effects, Atmos. Meas. Tech., 2, 33-46, 2009.

Formenti, P., Boucher, O., Reiner, T., Sprung, D., Andreae, M. O., Wendisch, M., Wex, H., Kindred, D., Tzortziou, M., and Vasaras, A.: STAAARTE-MED 1998 summer airborne measurements over the Aegean Sea 2. Aerosol scattering and absorption, and radiative calculations, Journal of Geophysical Research:

741 Atmospheres, 107, 2002.

742 Formenti, P., Mbemba Kabuiku, L., Chiapello, I., Ducos, F., Dulac, F., and Tanré, D.: Aerosol optical
743 properties derived from POLDER-3/PARASOL (2005–2013) over the western Mediterranean Sea: I.
744 Quality assessment with AERONET and in situ airborne observations, Atmos. Meas. Tech. Discuss.,
745 https://doi.org/10.5194/amt-2018-251, 2018.

746 Ghahremaninezhad, R., Norman, A.-L., Abbatt, J. P., Levasseur, M., and Thomas, J. L.: Biogenic,
747 anthropogenic and sea salt sulfate size-segregated aerosols in the Arctic summer, Atmospheric
748 Chemistry and Physics, 16, 5191-5202, 2016.

749 Haddad, I. E., D'Anna, B., Temime-Roussel, B., Nicolas, M., Boreave, A., Favez, O., Voisin, D., Sciare, J.,
750 George, C., and Jaffrezo, J.-L.: Towards a better understanding of the origins, chemical composition and
751 aging of oxygenated organic aerosols: case study of a Mediterranean industrialized environment,
752 Marseille, Atmospheric Chemistry and Physics, 13, 7875-7894, 2013.

753 Haywood, J., and Boucher, O.: Estimates of the direct and indirect radiative forcing due to tropospheric
754 aerosols: A review, Reviews of geophysics, 38, 513-543, 2000.

755 Healy, R. M., O'Connor, I. P., Hellebust, S., Allanic, A., Sodeau, J. R., & Wenger, J. C.:
756 Characterisation of single particles from in-port ship emissions. Atmospheric
757 Environment, 43(40), 6408-6414, 2009.

758 Hellmuth, O.: Columnar modelling of nucleation burst evolution in the convective boundary layer–first
759 results from a feasibility study Part IV: A compilation of previous observations for valuation of simulation
760 results from a columnar modelling study, Atmospheric Chemistry and Physics, 6, 4253-4274, 2006.

761 Hersey, S., Craven, J., Schilling, K., Metcalf, A., Sorooshian, A., Chan, M., Flagan, R., and Seinfeld, J.: The
762 Pasadena Aerosol Characterization Observatory (PACO): chemical and physical analysis of the Western
763 Los Angeles basin aerosol, Atmospheric Chemistry and Physics, 11, 7417-7443, 2011.

764 Hildebrandt, L., Engelhart, G., Mohr, C., Kostenidou, E., Lanz, V., Bougiatioti, A., DeCarlo, P., Prevot, A.,
765 Baltensperger, U., and Mihalopoulos, N.: Aged organic aerosol in the Eastern Mediterranean: the
766 Finokalia Aerosol Measurement Experiment–2008, Atmospheric Chemistry and Physics, 10, 4167-4186,
767 2010.

768 Hildebrandt, L., Kostenidou, E., Lanz, V., Prevot, A., Baltensperger, U., Mihalopoulos, N., Laaksonen, A.,
769 Donahue, N. M., and Pandis, S. N.: Sources and atmospheric processing of organic aerosol in the
770 Mediterranean: insights from aerosol mass spectrometer factor analysis, Atmospheric Chemistry and
771 Physics, 11, 12499-12515, 2011.

772 Isakson, J., Persson, T. A., & Lindgren, E. S.: Identification and assessment of ship emissions and their
773 effects in the harbour of Göteborg, Sweden. Atmospheric Environment, *35*(21), 3659-3666, 2001

774 Jimenez, J. L., Canagaratna, M., Donahue, N., Prevot, A., Zhang, Q., Kroll, J. H., DeCarlo, P. F., Allan, J. D.,
775 Coe, H., and Ng, N.: Evolution of organic aerosols in the atmosphere, Science, 326, 1525-1529, 2009.

776 Kalivitis, N., Stavroulas, I., Bougiatioti, A., Kouvarakis, G., Gagné, S., Manninen, H. E., Kulmala, M., and
777 Mihalopoulos, N.: Night-time enhanced atmospheric ion concentrations in the marine boundary layer,
778 Atmos. Chem. Phys., 12, 3627-3638, https://doi.org/10.5194/acp-12-3627-2012, 2012

779 Koçak, M., Mihalopoulos, N., and Kubilay, N.: Chemical composition of the fine and coarse fraction of
780 aerosols in the northeastern Mediterranean, Atmospheric Environment, 41, 7351-7368, 2007.

781 Koulouri, E., Saarikoski, S., Theodosi, C., Markaki, Z., Gerasopoulos, E., Kouvarakis, G., Mäkelä, T.,
782 Hillamo, R., and Mihalopoulos, N.: Chemical composition and sources of fine and coarse aerosol particles
783 in the Eastern Mediterranean, Atmospheric Environment, 42, 6542-6550, 2008.

784 Kulmala, M., Vehkamäki, H., Petäjä, T., Dal Maso, M., Lauri, A., Kerminen, V.-M., Birmili, W., and
785 McMurry, P.: Formation and growth rates of ultrafine atmospheric particles: a review of observations,
786 Journal of Aerosol Science, 35, 143-176, 2004.

787 Lanz, V. A., Alfarra, M. R., Baltensperger, U., Buchmann, B., Hueglin, C., Szidat, S., Wehrli, M. N., Wacker,
788 L., Weimer, S., and Caseiro, A.: Source attribution of submicron organic aerosols during wintertime
789 inversions by advanced factor analysis of aerosol mass spectra, Environmental Science & Technology,
790 42, 214-220, 2007.

791 Lauros, J., Nilsson, E., Maso, M. D., and Kulmala, M.: Contribution of mixing in the ABL to new particle
792 formation based on observations, Atmospheric Chemistry and Physics, 7, 4781-4792, 2007.

793 Lauros, J., Sogachev, A., Smolander, S., Vuollekoski, H., Sihto, S.-L., Mammarella, I., Laakso, L., Rannik, Ü.,
794 and Boy, M.: Particle concentration and flux dynamics in the atmospheric boundary layer as the
795 indicator of formation mechanism, Atmospheric Chemistry and Physics, 11, 5591-5601, 2011.

796 Lelieveld, J., Berresheim, H., Borrmann, S., Crutzen, P., Dentener, F., Fischer, H., Feichter, J., Flatau, P.,
797 Heland, J., and Holzinger, R.: Global air pollution crossroads over the Mediterranean, Science, 298, 794-
798 799, 2002.

799 Mallet, M., Dulac, F., Formenti, P., Nabat, P., Sciare, J., Roberts, G., Pelon, J., Ancellet, G., Tanré, D.,
800 Parol, F., Denjean, C., Brogniez, G., di Sarra, A., Alados-Arboledas, L., Arndt, J., Auriol, F., Blarel, L.,
801 Bourrianne, T., Chazette, P., Chevaillier, S., Claeys, M., D'Anna, B., Derimian, Y., Desboeufs, K., Di Iorio,
802 T., Doussin, J.-F., Durand, P., Féron, A., Freney, E., Gaimoz, C., Goloub, P., Gómez-Amo, J. L., Granados-
803 Muñoz, M. J., Grand, N., Hamonou, E., Jankowiak, I., Jeannot, M., Léon, J.-F., Maillé, M., Mailler, S.,
804 Meloni, D., Menut, L., Momboisse, G., Nicolas, J., Podvin, T., Pont, V., Rea, G., Renard, J.-B., Roblou, L.,
805 Schepanski, K., Schwarzenboeck, A., Sellegri, K., Sicard, M., Solmon, F., Somot, S., Torres, B., Totems, J.,
806 Triquet, S., Verdier, N., Verwaerde, C., Waquet, F., Wenger, J., and Zapf, P.: Overview of the Chemistry-
807 Aerosol Mediterranean Experiment/ Aerosol Direct Radiative Forcing on the Mediterranean Climate
808 (ChArMEx/ADRIMED) summer 2013 campaign, Atmos. Chem. Phys., 16, 455–504, 2016.

809 Mariotti, A., Pan, Y., Zeng, N., and Alessandri, A.: Long-term climate change in the Mediterranean region
810 in the midst of decadal variability, Climate Dynamics, 44, 1437-1456, 2015.

811 Meloni, D., di Sarra, A., Pace, G., and Monteleone, F.: Aerosol optical properties at Lampedusa (Central

812 Mediterranean). 2. Determination of single scattering albedo at two wavelengths for different aerosol
813 types, Atmospheric Chemistry and Physics, 6, 715-727, 2006.

814 Michoud, V., Sciare, J., Sauvage, S., Dusanter, S., Léonardis, T., Gros, V., Kalogridis, C., Zannoni, N., Féron,
815 A., and Petit, J.-E.: Organic carbon at a remote site of the western Mediterranean Basin: sources and
816 chemistry during the ChArMEx SOP2 field experiment, Atmospheric chemistry and physics, 17, 8837-
817 8865, 2017.

818 Middlebrook, A., Bahreini, R., Jiminez, J., and Canagaratna, M.: Evaluation of composition-dependent
819 collection efficiencies for the aerodyne aerosol mass spectrometer using field data, Atmospheric
820 Chemistry and Physics, 46, 258-271, 2012

821 Minguillón, M., Pérez, N., Marchand, N., Bertrand, A., Temime-Roussel, B., Agrios, K., Szidat, S., van
822 Drooge, B., Sylvestre, A., and Alastuey, A.: Secondary organic aerosol origin in an urban environment:
823 influence of biogenic and fuel combustion precursors, Faraday Discuss, 189, 337-359, 2016.

824 Minguillón, M. C., Ripoll, A., Pérez, N., Prévôt, A., Canonaco, F., Querol, X., and Alastuey, A.: Chemical
825 characterization of submicron regional background aerosols in the western Mediterranean using an
826 Aerosol Chemical Speciation Monitor, Atmospheric Chemistry and Physics, 15, 6379-6391, 2015.

827 Mohr, C., DeCarlo, P., Heringa, M., Chirico, R., Slowik, J., Richter, R., Reche, C., Alastuey, A., Querol, X.,
828 and Seco, R.: Identification and quantification of organic aerosol from cooking and other sources in
829 Barcelona using aerosol mass spectrometer data, Atmospheric Chemistry and Physics, 12, 1649-1665,
830 2012.

831 Muller, M., George, C., and D'Anna, B.: Enhanced spectral analysis of C-TOF Aerosol Mass Spectrometer
832 data: iterative residual analysis and cumulative peak fitting, International Journal of Mass Spectrometry,
833 306, 1-8, 2011.

834 Ng, N., Canagaratna, M., Zhang, Q., Jimenez, J., Tian, J., Ulbrich, I., Kroll, J., Docherty, K., Chhabra, P., and
835 Bahreini, R.: Organic aerosol components observed in Northern Hemispheric datasets from Aerosol
836 Mass Spectrometry, Atmospheric Chemistry and Physics, 10, 4625-4641, 2010.

837 Ng, N., Canagaratna, M., Jimenez, J., Chhabra, P., Seinfeld, J., and Worsnop, D.: Changes in organic
838 aerosol composition with aging inferred from aerosol mass spectra, Atmospheric Chemistry and Physics,
839 11, 6465-6474, 2011.

840 Orsini, D. A., Ma, Y., Sullivan, A., Sierau, B., Baumann, K., and Weber, R. J.: Refinements to the particle-
841 into-liquid sampler (PILS) for ground and airborne measurements of water soluble aerosol composition,
842 Atmospheric Environment, 37, 1243-1259, 2003.

843 Ortiz-Amezcua, P., Guerrero-Rascado, J., Granados-Muñoz, M., Bravo-Aranda, J., and Alados-Arboledas,
844 L.: Characterization of atmospheric aerosols for a long range transport of biomass burning particles from
845 canadian forest fires over the southern iberian peninsula in July 2013, Optica Pura y Aplicada, 47, 43-49,
846 2014.

847 Ovadnevaite, J., Ceburnis, D., Canagaratna, M., Berresheim, H., Bialek, J., Martucci, G., Worsnop, D. R.,

and O'Dowd, C.: On the effect of wind speed on submicron sea salt mass concentrations and source fluxes, Journal of Geophysical Research: Atmospheres (1984–2012), 117, 2012.

Paatero, P., and Tapper, U.: Positive matrix factorization: A non-negative factor model with optimal utilization of error estimates of data values, Environmetrics, 5, 111-126, 1994.

Paatero, P.: Least squares formulation of robust non-negative factor analysis, Chemometrics and Intelligent Laboratory Systems, 37, 23-35, 1997.

Pace, G., Meloni, D., and di Sarra, A.: Forest fire aerosol over the Mediterranean basin during summer 2003, Journal of Geophysical Research: Atmospheres, 110, 2005.

Pace, G., Meloni, D., and di Sarra, A.: Forest fire aerosol over the Mediterranean basin during summer 2003, Journal of Geophysical Research: Atmospheres, 110, D21202, doi:10.1029/2005JD005986, 2005.

Pace, G., di Sarra, A., Meloni, D., Piacentino, S., and Chamard, P.: Aerosol optical properties at Lampedusa (Central Mediterranean). 1. Influence of transport and identification of different aerosol types, Atmospheric Chemistry and Physics, 6, 697-713, 2006.

Perrone, M., and Bergamo, A.: Direct radiative forcing during Sahara dust intrusions at a site in the Central Mediterranean: Anthropogenic particle contribution, Atmospheric Research, 101, 783-798, 2011.

Perrone, M., Becagli, S., Orza, J. G., Vecchi, R., Dinoi, A., Udisti, R., and Cabello, M.: The impact of long-range-transport on PM1 and PM2. 5 at a Central Mediterranean site, Atmospheric environment, 71, 176-186, 2013.

Petit, J.-E., Favez, O., Albinet, A., and Canonaco, F.: A user-friendly tool for comprehensive evaluation of the geographical origins of atmospheric pollution: Wind and trajectory analyses, Environmental Modelling & Software, 88, 183-187, 2017.

Pikridas, M., Riipinen, I., Hildebrandt, L., Kostenidou, E., Manninen, H., Mihalopoulos, N., Kalivitis, N., Burkhart, J. F., Stohl, A., and Kulmala, M.: New particle formation at a remote site in the eastern Mediterranean, Journal of Geophysical Research: Atmospheres, 117, 2012.

Querol, X., Alastuey, A., Pey, J., Cusack, M., Pérez, N., Mihalopoulos, N., Theodosi, C., Gerasopoulos, E., Kubilay, N., and Koçak, M.: Variability in regional background aerosols within the Mediterranean, Atmospheric Chemistry and Physics, 9, 4575-4591, 2009a.

Querol, X., Pey, J., Pandolfi, M., Alastuey, A., Cusack, M., Pérez, N., Moreno, T., Viana, M., Mihalopoulos, N., and Kallos, G.: African dust contributions to mean ambient PM10 mass-levels across the Mediterranean Basin, Atmospheric Environment, 43, 4266-4277, 2009b.

Rinaldi, M., Gilardoni, S., Paglione, M., Sandrini, S., Decesari, S., Zanca, N., Marinoni, A., Cristofanelli, P., Bonasoni, P., and Ielpo, P.: Physico-chemical characterization of Mediterranean background aerosol at the Capogranitola observatory (Sicily), EGU General Assembly Conference Abstracts, 2017, 3161.

882 Sanchez-Gomez, E., Somot, S., and Mariotti, A.: Future changes in the Mediterranean water budget
883 projected by an ensemble of regional climate models, Geophysical Research Letters, 36, 2009.

884 Schembari, C., Bove, M., Cuccia, E., Cavalli, F., Hjorth, J., Massabò, D., Nava, S., Udisti, R., and Prati, P.:
885 Source apportionment of PM10 in the Western Mediterranean based on observations from a cruise
886 ship, Atmospheric environment, 98, 510-518, 2014.

887 Schmale, J., Schneider, J., Nemitz, E., Tang, Y., Dragosits, U., Blackall, T., Trathan, P., Phillips, G., Sutton,
888 M., and Braban, C.: Sub-Antarctic marine aerosol: dominant contributions from biogenic sources,
889 Atmospheric Chemistry and Physics, 13, 8669-8694, 2013.

890 Sciare, J., Bardouki, H., Moulin, C., and Mihalopoulos, N.: Aerosol sources and their contribution to the
891 chemical composition of aerosols in the Eastern Mediterranean Sea during summertime, Atmospheric
892 Chemistry and Physics, 3, 291-302, 2003.

893 Sciare, J., Oikonomou, K., Favez, O., Liakakou, E., Markaki, Z., Cachier, H., and Mihalopoulos, N.: Long-
894 term measurements of carbonaceous aerosols in the Eastern Mediterranean: evidence of long-range
895 transport of biomass burning, Atmospheric Chemistry and Physics, 8, 5551-5563, 2008.

896 Siebert, H., Wehner, B., Hellmuth, O., Stratmann, F., Boy, M., and Kulmala, M.: New-particle formation
897 in connection with a nocturnal low-level jet: Observations and modeling results, Geophysical Research
898 Letters, 34, 2007.

899 Sirois, A., and Bottenheim, J. W.: Use of backward trajectories to interpret the 5-year record of PAN and
900 O3 ambient air concentrations at Kejimkujik National Park, Nova Scotia, Journal of Geophysical
901 Research: Atmospheres, 100, 2867-2881, 1995.

902 Stein, A., Draxler, R. R., Rolph, G. D., Stunder, B. J., Cohen, M., and Ngan, F.: NOAA's HYSPLIT
903 atmospheric transport and dispersion modeling system, Bulletin of the American Meteorological
904 Society, 96, 2059-2077, 2015.

905 Stohl, A., Forster, C., Frank, A., Seibert, P., and Wotawa, G.: The Lagrangian particle dispersion model
906 FLEXPART version 6.2, Atmospheric Chemistry and Physics, 5, 2461-2474, 2005.

907 Stratmann, F., Siebert, H., Spindler, G., Wehner, B., Althausen, D., Heintzenberg, J., Hellmuth, O., Rinke,
908 R., Schmieder, U., and Seidel, C.: New-particle formation events in a continental boundary layer: first
909 results from the SATURN experiment, Atmospheric Chemistry and Physics, 3, 1445-1459, 2003.

910 Tadros, C. V., Crawford, J., Treble, P. C., Baker, A., Cohen, D. D., Atanacio, A. J., Hankin, S., and Roach, R.:
911 Chemical characterisation and source identification of atmospheric aerosols in the Snowy Mountains,
912 south-eastern Australia, Science of The Total Environment, 630, 432-443, 2018.

913 Ulbrich, I., Canagaratna, M., Zhang, Q., Worsnop, D., and Jimenez, J.: Interpretation of organic
914 components from Positive Matrix Factorization of aerosol mass spectrometric data, Atmospheric
915 Chemistry and Physics, 9, 2891-2918, 2009.

916 Wehner, B., Siebert, H., Ansmann, A., Ditas, F., Seifert, P., Stratmann, F., Wiedensohler, A., Apituley, A.,

Shaw, R., and Manninen, H.: Observations of turbulence-induced new particle formation in the residual layer, Atmospheric chemistry and physics, 10, 4319-4330, 2010.

World Health Organization.: Ambient air pollution: A global assessment of exposure and burden of disease, 2016.

Zhang, H., Surratt, J., Lin, Y., Bapat, J., and Kamens, R.: Effect of relative humidity on SOA formation from isoprene/NO photooxidation: enhancement of 2-methylglyceric acid and its corresponding oligoesters under dry conditions, Atmospheric Chemistry and Physics, 11, 6411-6424, 2011.

Zhang, Q., Worsnop, D., Canagaratna, M., and Jimenez, J. L.: Hydrocarbon-like and oxygenated organic aerosols in Pittsburgh: insights into sources and processes of organic aerosols, Atmospheric Chemistry and Physics, 5, 3289-3311, 2005.

Zhang, Q., Jimenez, J. L., Canagaratna, M. R., Allan, J. D., Coe, H., Ulbrich, I., Alfarra, M. R., Takami, A., Middlebrook, A. M., Sun, Y. L., Dzepina, K., Dunlea, E., Docherty, K., DeCarlo, P. F., Salcedo, D., Onasch, T., Jayne, J. T., Miyoshi, T., Shimono, A., Hatakeyama, S., Takegawa, N., Kondo, Y., Schneider, J., Drewnick, F., Borrmann, S., Weimer, S., Demerjian, K., Williams, P., Bower, K., Bahreini, R., Cottrell, L., Griffin, R. J., Rautiainen, J., Sun, J. Y., Zhang, Y. M., and Worsnop, D. R.: Ubiquity and dominance of oxygenated species in organic aerosols in anthropogenically-influenced Northern Hemisphere midlatitudes, Geophys. Res. Lett., 34, L13801, doi:10.1029/2007GL029979, 2007.

Zhou, S., Collier, S., Xu, J., Mei, F., Wang, J., Lee, Y. N., Sedlacek, A. J., Springston, S. R., Sun, Y., and Zhang, Q.: Influences of upwind emission sources and atmospheric processing on aerosol chemistry and properties at a rural location in the Northeastern US, Journal of Geophysical Research: Atmospheres, 121, 6049-6065, 2016.

Figure 1 The Mediterranean basin. The two sites considered in this study, Lampedusa and Ersa, are indicated with white dots. Image is courtesy of Google Earth.

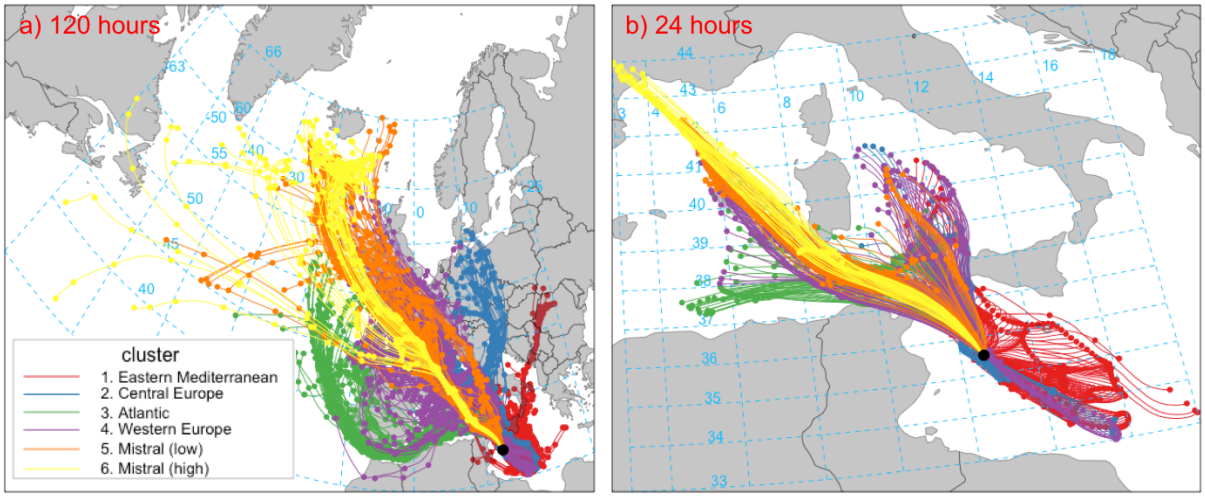

Figure 2 a) Hourly 144-hour (6 days) backwards trajectories from Lampedusa from 10 June 2013 until 5 July 2013, cut off at 120 hours (5 days). Colours represent the assigned cluster. B) The same as a) but cut off at 24-hour.

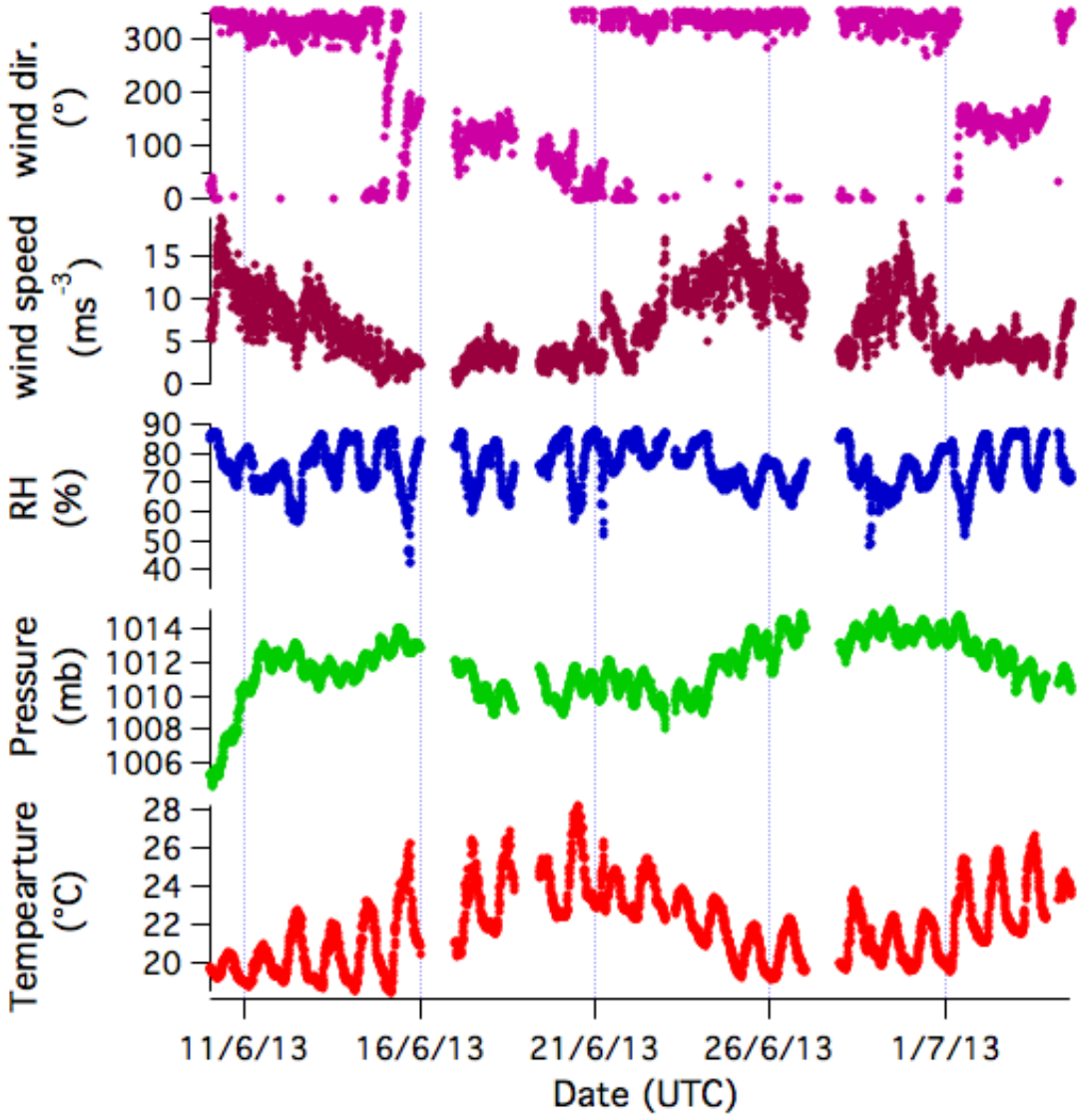

Figure 3 Meteorological conditions (wind direction and speed, relative humidity, pressure and temperature) measured at the Lampedusa site during SOP-1a.

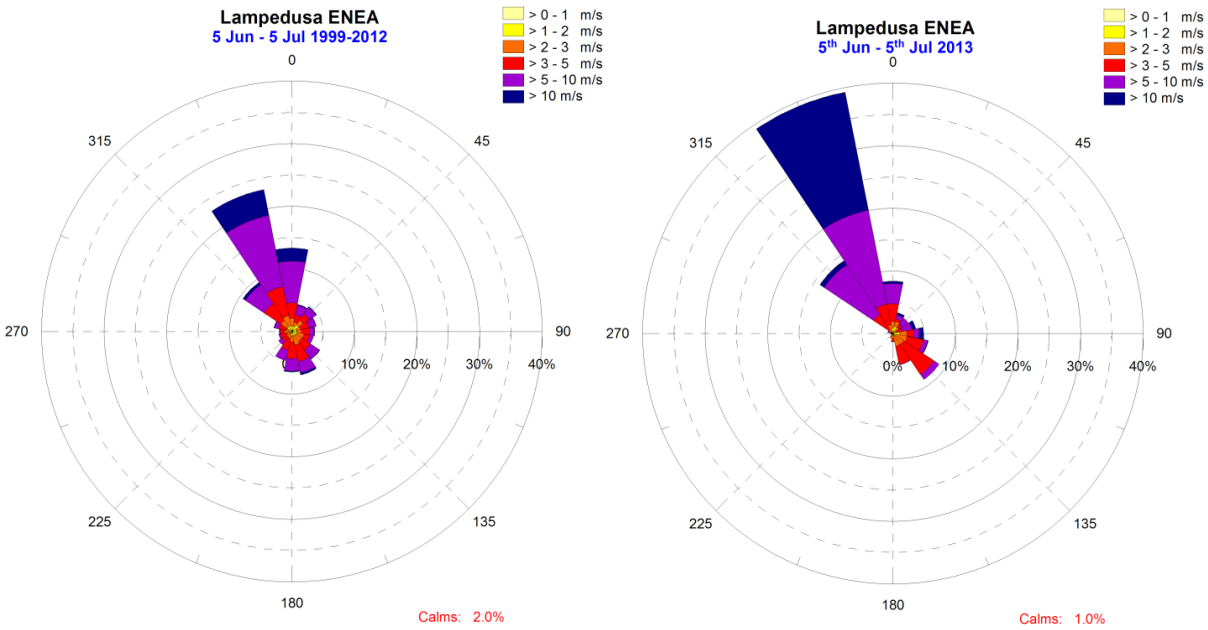

Figure 4 Wind speed and direction at Lampedusa during the period from 5 June until 5 July during the years from 1999 - 2012 (left) and during this campaign (right).

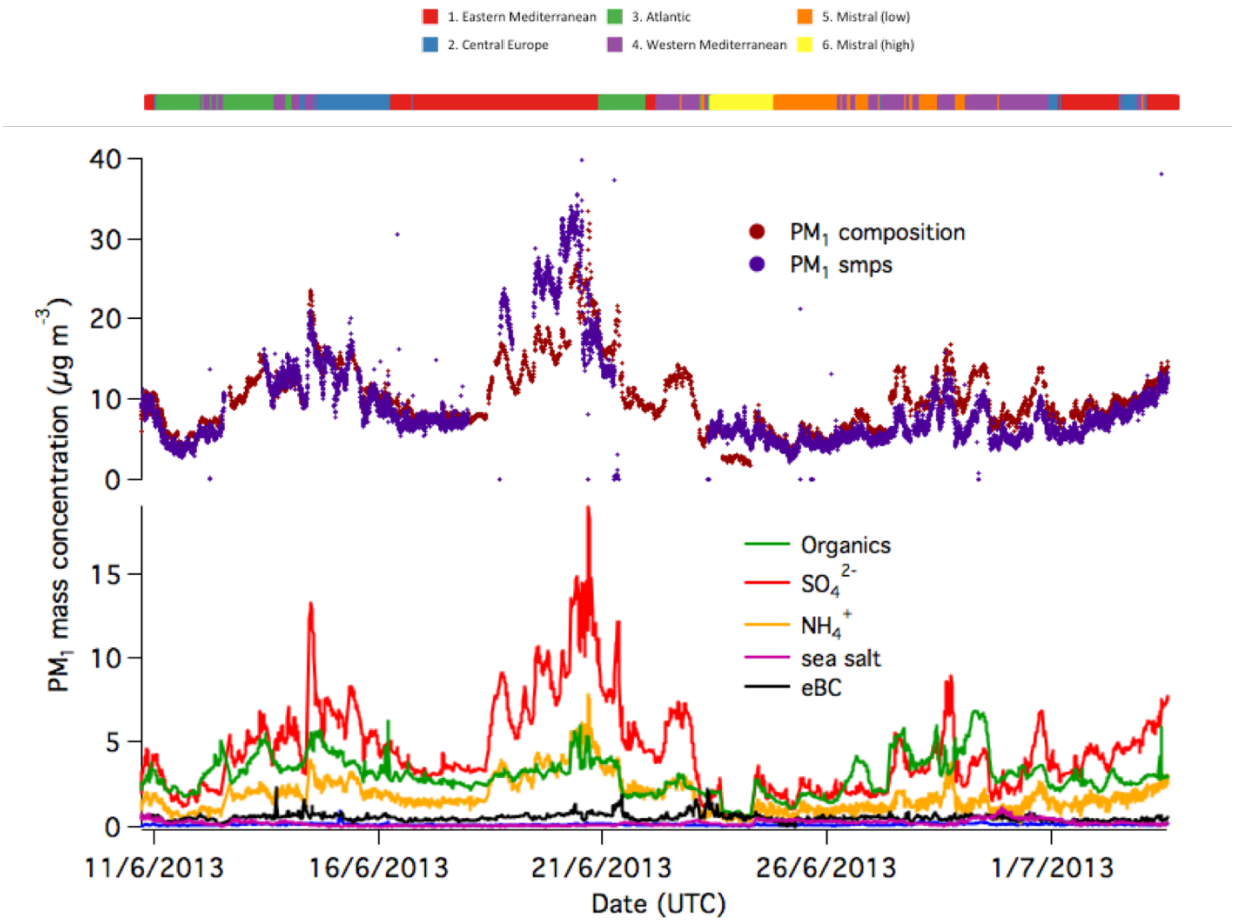

Figure 5 The time series of PM_1 mass concentration, coloured by the relative contribution from each species. The top bar is coloured according to the air mass origin.

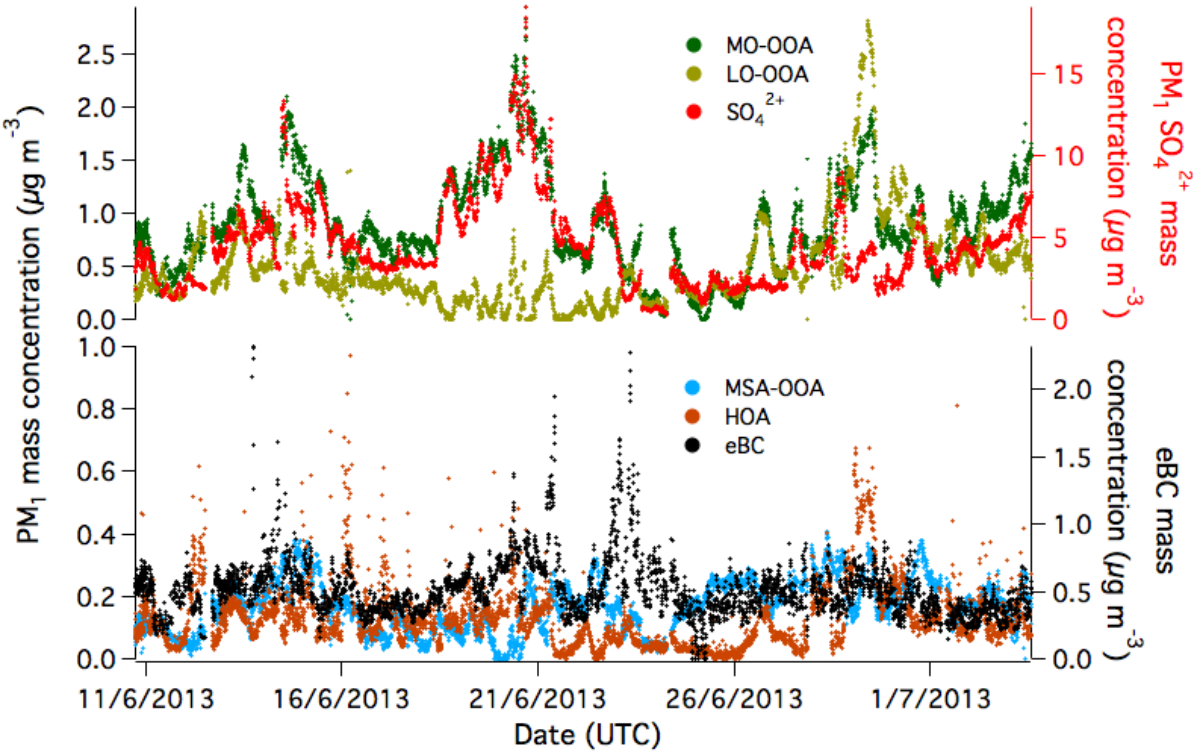

Figure 6 The time series of the PM_1 "more oxidised" OOA (MO-OOA), "less oxidised" (LO-OOA) and sulphate (top panel) and methanesulfonic acid-related OOA (MSA-OOA), hydrocarbon-like OA (HOA) and eBC (bottom panel).

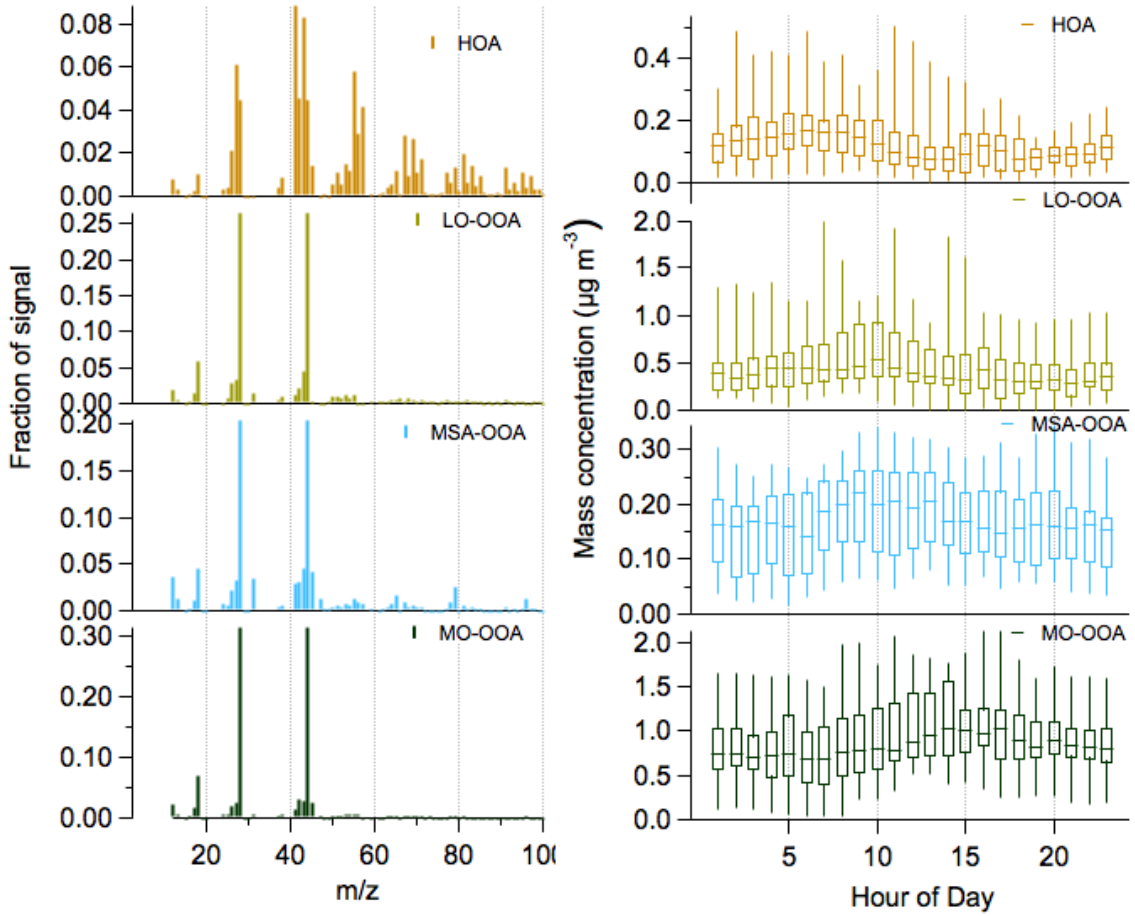

Figure 7 The mass spectra for the 4 PMF factors (HOA: hydrocarbon-like organic aerosol, LO-OOA: less oxidised OOA, MO-OOA: more oxidised OOA, MSA-OOA: methanesulfonic acid-related OOA) retrieved from the PMF analysis of unit-mass resolution data.

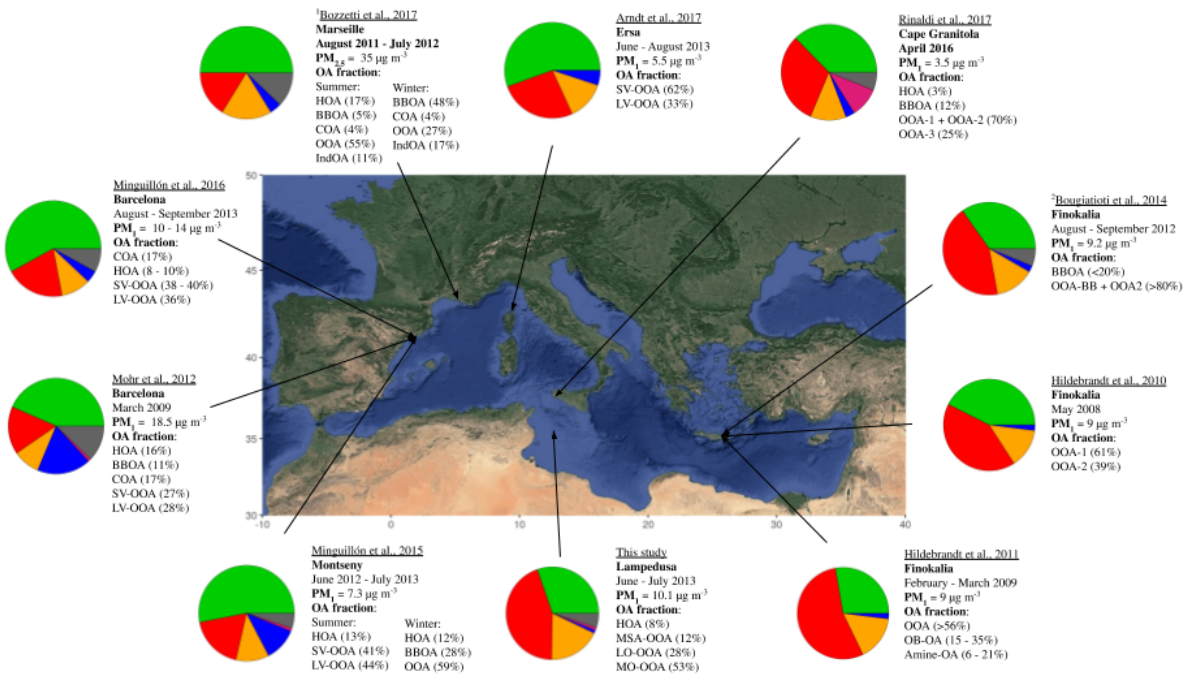

Figure 8 A summary of studies that have investigated NR-PM$_1$ composition (including PMF of OA) around the Mediterranean basin. Only studies that have investigated PMF-based OA source apportionment are reported. Pie charts display the average concentration during each study where green corresponds to organics, red to sulphates, orange to ammonium, blue to nitrate, pink to either chlorides or sea salt and black to elemental or black carbon. The OA fraction acronyms correspond to the following:HOA: Hydrocarbon-like Organic Aerosol, SV-OOA: Semi-volatile oxygenated Organic Aerosol, LV-OOA: Low-volatility oxygenated Organic Aerosol, BBOA: Biomass burning Organic Aerosol, COA: Cooking Organic Aerosol, OOA: Oxygenated Organic Aerosol, F4: "Factor -4" (unidentified PMF factor), IndOA: Industry-related Organic Aerosol, OB-OA: "Olive-branch Organic Aerosol. See Supplementary Tables S1 and S2 for further details about the sampling locations, instruments used and pie chart values. [1]This study collected on PM2.5 filters and nebulised into an HR-ToF-AMS. [2]Excludes fire-periods.

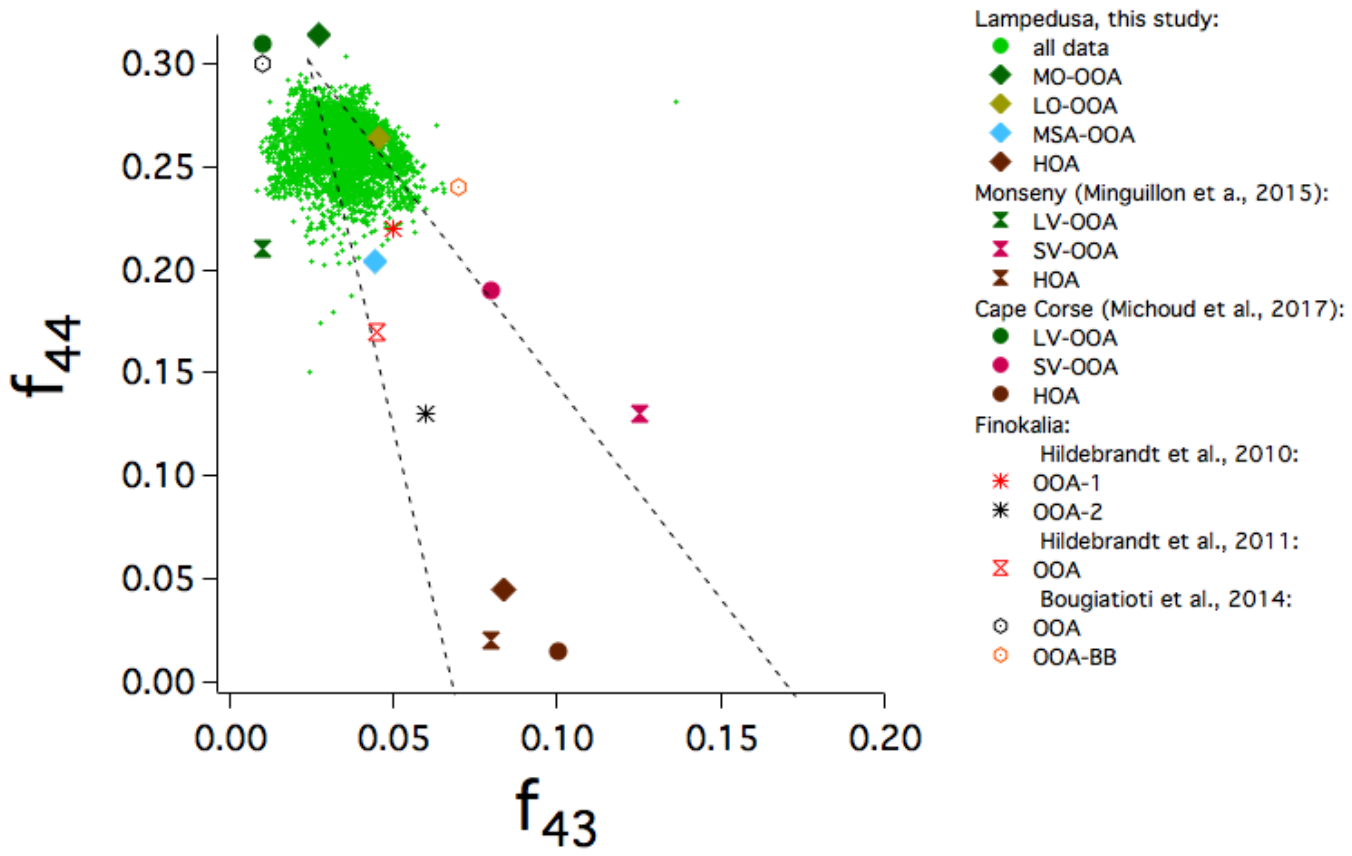

Figure 9 f_{43} (the ratio of m/z 43 to the total OA) against f_{44} (ratio of m/z 44 to the total OA). The triangle is considered to encapsulate typical atmospheric values of OA according to Ng et al. (2010). The values for the various PMF factors from this study and other studies conducted in the remote Mediterranean are also displayed.

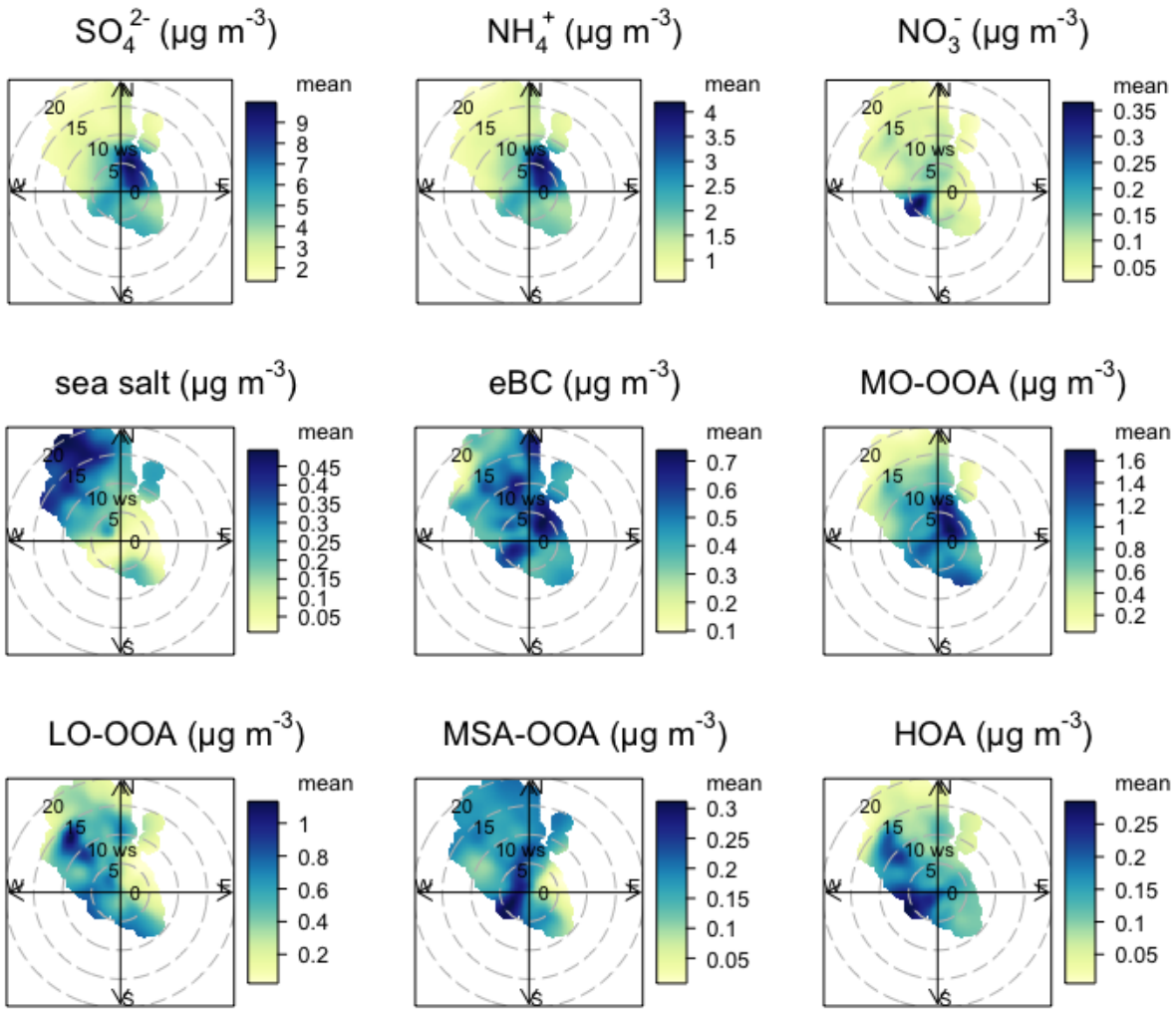

Figure 10 Bi-variate polar plots of mean concentrations of PM_1 species and f_{44} at Lampedusa. The angle represents the arrival wind direction, the radius represents the wind speed and the colours represent the mean concentrations for the respective wind directions and winds.

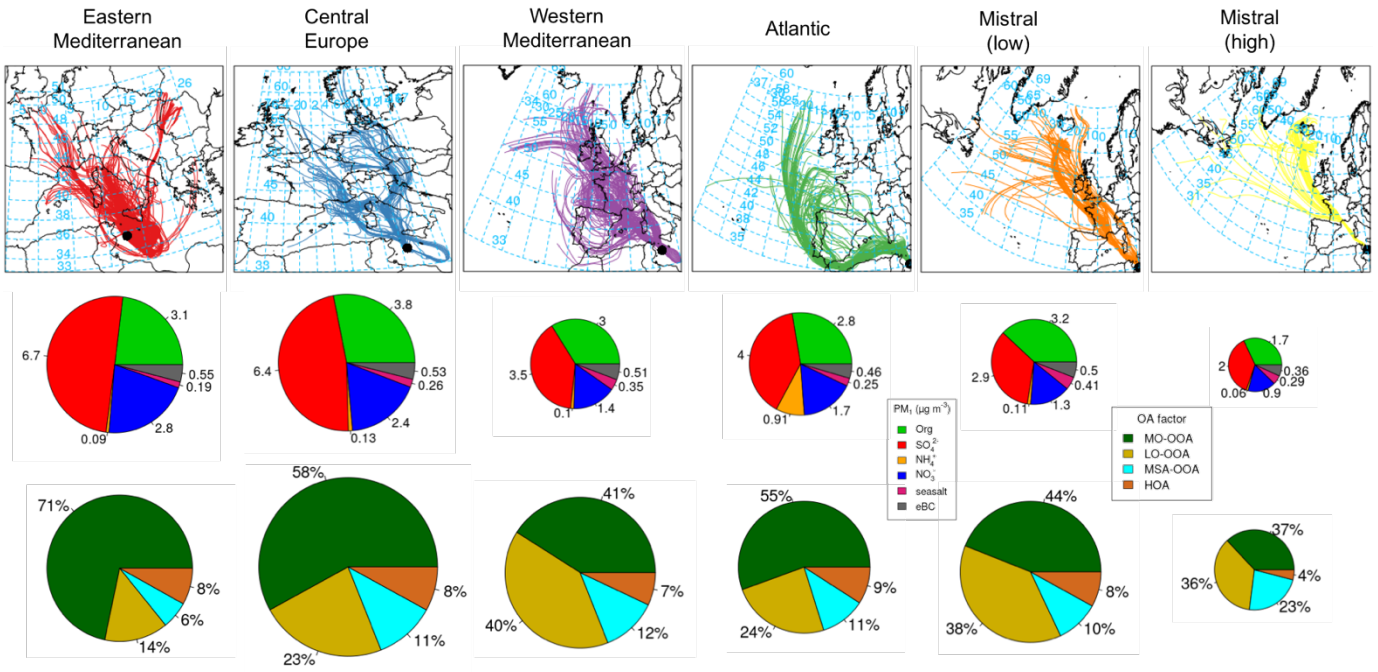

Figure 11 top) 144 hour air mass back trajectories, assigned to each cluster; middle) the PM_1 composition for each air mass cluster and bottom) the contribution of OA factors for each air mass cluster. The diameter for the PM_1 composition pie graphs are proportional to the total PM_1 concentration for each air mass cluster period and the radius for the OA factor pie graphs is proportional to the total PM_1 organic concentration for each air mass cluster period.

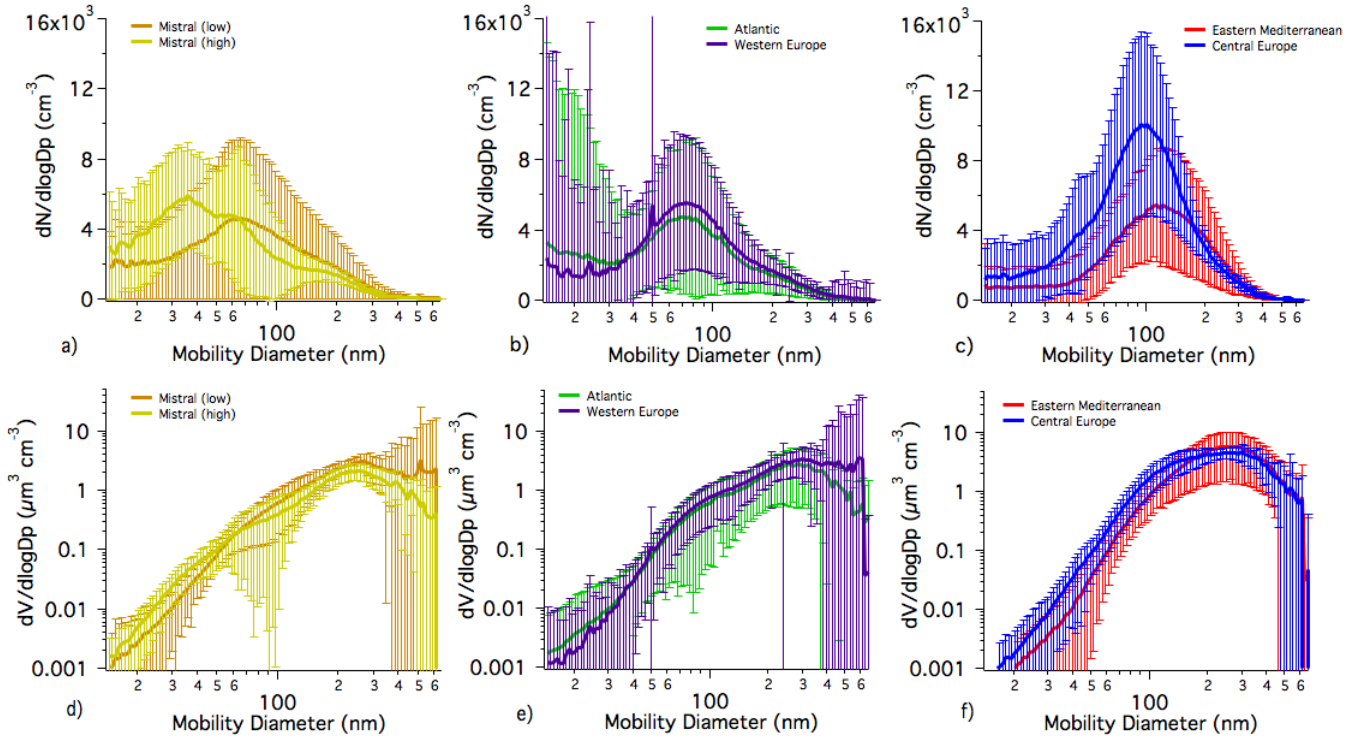

Figure 12 The number size distribution of PM_1 aerosol, coloured by averages for different air mass origin: a) Mistral (high) and Mistral (low); b) Atlantic and Western Europe; c) Eastern Mediterranean and Central Europe and the

volume size distribution of PM_1 aerosol, coloured by averages for different air mass origin: d) Mistral (high) and Mistral (low); e) Atlantic and Western Europe; f) Eastern Mediterranean and Central Europe.

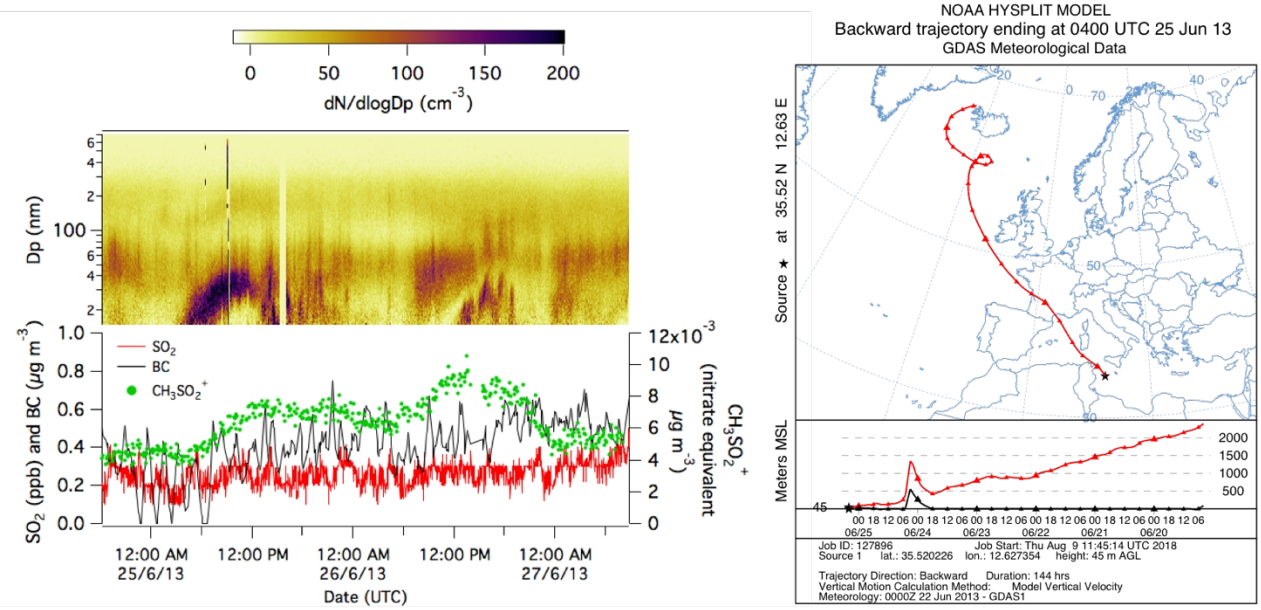

Figure 13 (left) The number size distribution during a new particle formation event on 25 June 2013 and the corresponding concentrations of SO_2, eBC and MSA fragment, $CH_3SO_2^+$, and (right) the HYSPLIT air mass backwards trajectory during the event.

Table 1 Campaign average PM_1 concentration for the major aerosol species measured at the Ersa and Lampedusa sites during the SOP-1a period and for periods of coincident air mass backwards trajectories between Ersa and Lampedusa

SITE	SO_4^{2-}	ORGANIC	NH_4^+	NO_3^-
ERSA	1.4 ± 2.6	3.0 ± 1.1	0.7 ± 1	0.3 ± 0.1
LAMPEDUSA	4.5 ± 0.9	3.0 ± 1.6	1.9 ± 0.5	0.1 ± 0.2
ERSA (COINCIDENT WITH LAMPEDUSA)	0.9 ± 0.5	2.7 ± 1.1	0.5 ± 0.3	0.4 ± 0.3
LAMPEDUSA (COINCIDENT WITH ERSA)	5.3 ± 2.0	3.8 ± 0.8	2.0 ± 0.6	0.1 ± 0.1

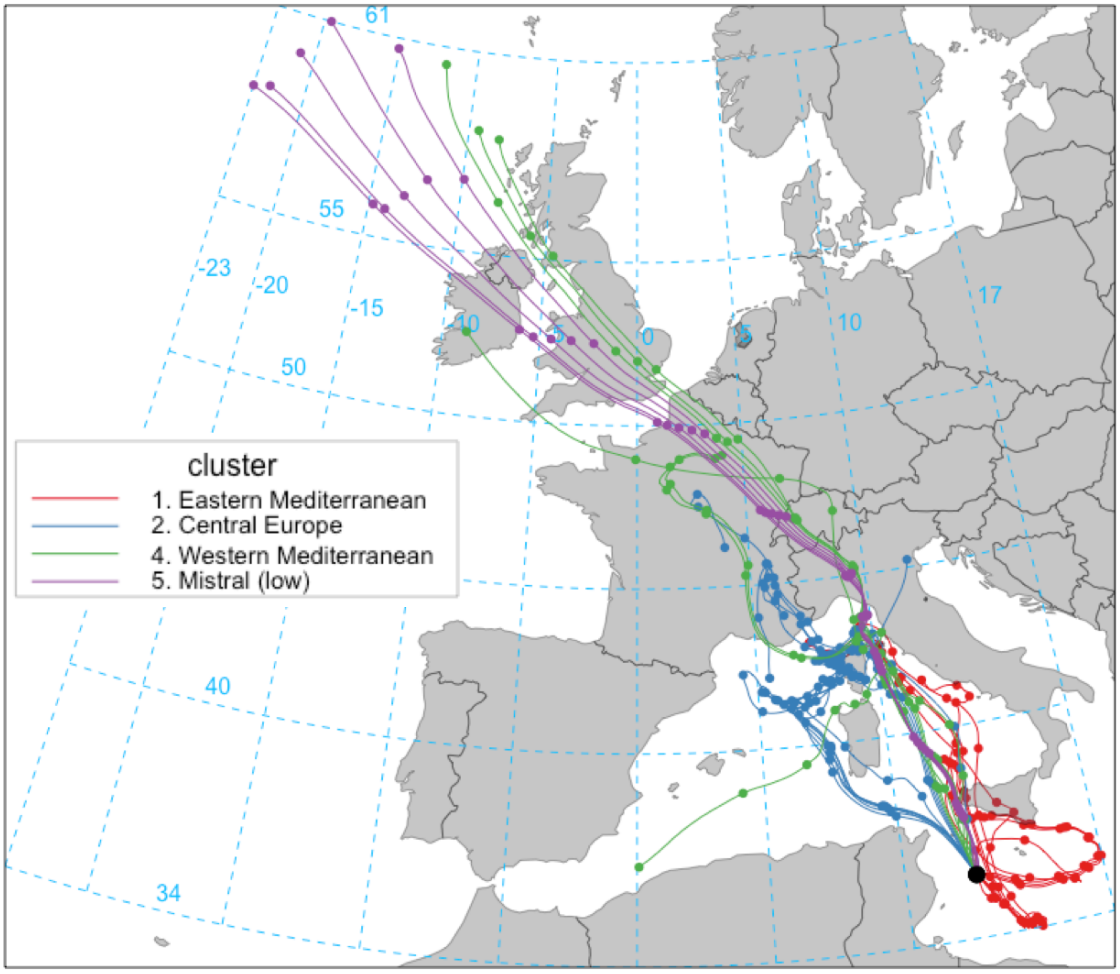

Figure 14 Hourly 120-hour (5 days) backwards trajectories from Lampedusa that passed within ±1° in latitude and longitude and ±200 m in altitude of the Ersa station. The colours represent the assigned cluster (performed on 144 hour trajectories).

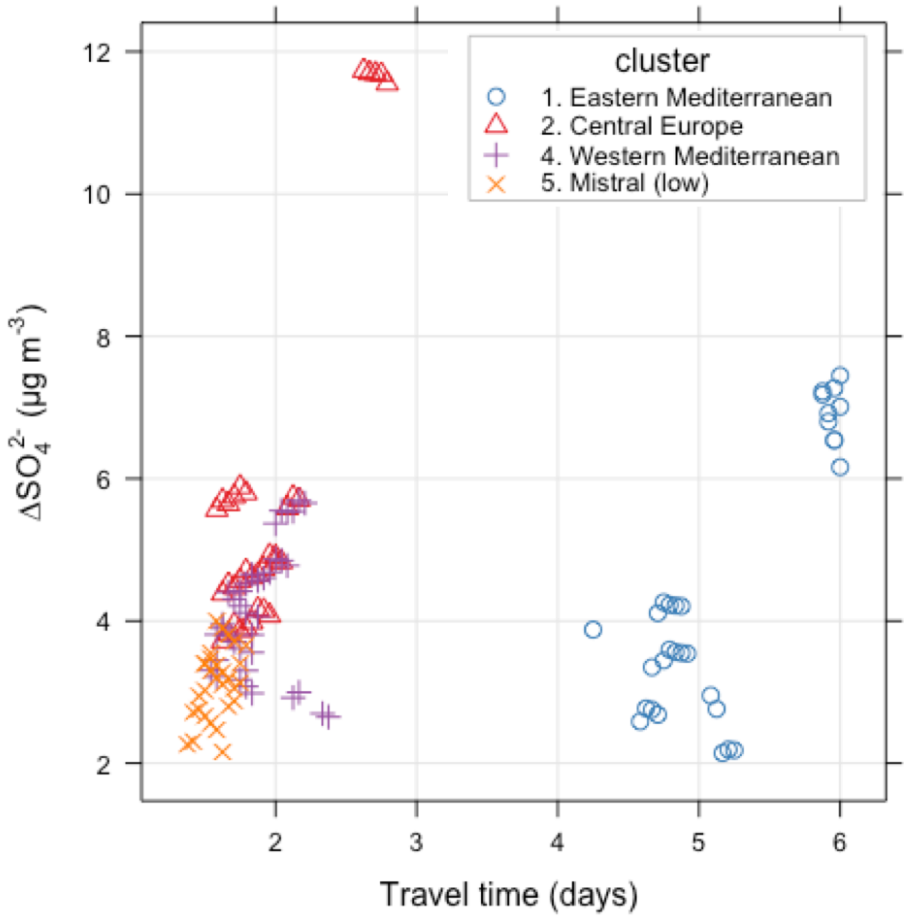

Figure 15 The difference in the PM_1 SO_4^{2-} mass concentration at Lampedusa and Ersa as a function of the travel time of the air masses from Ersa to Lampedusa. Colours represent the air mass origin cluster.